Neoproterozoic–Paleozoic detrital sources in the Variscan foreland of northern Iberia: primary v. recycled sediments

G. Gutiérrez-Alonso[1,2]*, A. López-Carmona[1,2], E. Núñez-Guerrero[1],
A. Martínez García[1], J. Fernández-Suárez[3,4], D. Pastor-Galán[5],
J. C. Gutiérrez-Marco[4], E. Bernárdez[6], J. R. Colmenero[1], M. Hofmann[7] and
U. Linnemann[7]

[1]Geology Department, Faculty of Science, University of Salamanca, Plaza de la Merced s/n, 37008, Salamanca, Spain

[2]Laboratory of Structural Petrology, Faculty of Geology and Geography, Tomsk State University, 36 Lenin Avenue, 634050, Tomsk, Russia

[3]Mineralogy and Petrology Department, Faculty of Geology, Complutense University of Madrid; Calle José Antonio Novais, 12, 28040 Madrid, Spain

[4]Instituto de Geociencias (CSIC, UCM), 28040 Madrid, Spain

[5]CNEAS, Tohoku University, 41 Kawauchi, Aoba-ku, Sendai, Japan

[6]INSUGEO Sede Miguel Lillo, Miguel Lillo 205 (CP 4000) San Miguel de Tucumán, Argentina

[7]Senckenberg Naturhistorische Sammlungen Dresden, Museum für Mineralogie und Geologie, Sektion Geochronologie, Königsbrücker Landstraße 159, 01109 Dresden, Germany

GG-A, 0000-0002-4370-4580; AL-C, 0000-0002-2513-6559;
EN-G, 0000-0003-2829-9422; DP-G, 0000-0002-0226-2739;
JCG-M, 0000-0003-4213-6144; EB, 0000-0001-5114-2592; MH, 0000-0003-0027-5349
*Correspondence: gabi@usal.es

Abstract: The Cantabrian Zone, in the Variscan belt of Western Europe, has one of the most continuous Ediacaran–Paleozoic stratigraphic successions in the world. This succession has been extensively studied, including several detrital zircon U–Pb geochronological studies on 30 samples spanning the aforementioned time slice. In this work, we present data from three new samples covering previously unsampled time-slices and perform multidimensional analysis on the 33 samples in order to quantify the similarity/dissimilarity among all of them with the aim of detecting potential changes in source areas through time and the role of recycling. The results indicate a continuous source of sediments from Ediacaran to late Devonian times punctuated by a sudden ephemeral change in the Early Cambrian that can be attributed to local causes during the inception of the Paleozoic passive margin.

Over the past two decades, U–Pb dating of detrital zircon grains in (meta) sedimentary rocks has become a powerful tool to investigate palaeogeographic, tectonic and provenance scenarios in geological realms at different scales (e.g. Fernández-Suárez *et al.* 2000, 2014; Martínez Catalán *et al.* 2004; Murphy *et al.* 2004*a*; Mazur *et al.* 2010; Henderson *et al.* 2016; Žák and Sláma 2018; Stephan *et al.* 2019). Although most studies based on detrital zircon geochronology are focused on constraining provenance and palaeogeographic affinities, when detrital zircon age data are available for continuous sedimentary formations covering a wide time span in the same region, these data can also provide a more dynamic view, helping to constrain the geological evolution of the area at different scales.

The sedimentary rocks in the northern Gondwana margin record a protracted geological history that began with subduction and arc construction in Ediacaran times followed by the establishment of a long-lived and complex passive margin that underwent several episodes of extension (e.g. Gutiérrez-Marco *et al.* 2019). This passive margin was eventually involved in the late Devonian to Carboniferous Variscan collision between Gondwana and Laurussia (e.g. Matte 1986; Martínez Catalán *et al.* 2007, 2019; Hibbard *et al.* 2010) that produced the amalgamation of Pangaea and the subsequent generation of the Ibero-Armorican Orocline (Weil *et al.* 2013).

The Cantabrian Zone, the Variscan foreland fold and thrust belt in the Iberian Massif is one of the best preserved and exposed sedimentary records of the

northern Gondwanan margin (Fig. 1), where the stratigraphic sequence contains an almost complete succession from Ediacaran to Permian times, spanning *c.* 300 Ma that include supercontinent breakup and amalgamation, from Pannotia to Pangaea (e.g. Nance and Murphy 2019). Detrital zircon geochronology has been intensively applied to these formations since the advent of laser ablation U–Pb dating (U–Pb laser ablation with inductively coupled plasma mass spectrometry, LA–ICP–MS) and there is now an extensive dataset (30 studied samples, Fernández-Suárez *et al.* 2000, 2002*a*, *b*, 2014; Gutiérrez-Alonso *et al.* 2003, 2015; Pastor-Galán *et al.* 2013*a*; Shaw *et al.* 2014; Zimmermann *et al.* 2015; Henderson *et al.* 2016; Naidoo *et al.* 2018). These samples provide a complete Ediacaran–Paleozoic history constraining provenance changes and recycling, which can be linked to different tectonic events at different scales.

The recent use of statistical tools to quantify the similarity/dissimilarity between different detrital zircon populations (e.g. Vermeesch 2013, 2017, 2018; Saylor and Sundell 2016; Andersen *et al.* 2018), instead of making comparisons by mere visual inspection of probability density plots

(PDPs) or kernel density estimations (KDEs), provides new insights into changes in sedimentary sources and the role of recycling through time, the latter being particularly relevant when orogenic processes occur. Given the large number of samples studied in the Cantabrian Zone and their distribution in time, this region is ideal to perform quantitative statistical analyses and obtain further insight into correspondence between the geological evolution of the area and the features of the detrital zircon age populations.

In this paper, we present zircon ages for three new samples of Ordovician and Devonian age that complete some sampling gaps in previous studies. Using the published (see above) and new data, we performed a multidimensional scaling analysis (MDS; Vermeesch 2013) on the dataset. With multidimensional scaling we attempt a correlation of the similarity/dissimilarity among the samples with the geological history of the region and the processes inferred from the regional geology. From this analysis, changes in sediment sources and the most important tectonic events in the Cantabrian Zone can be detected and documented, from large to local-scale tectonics to sedimentary recycling.
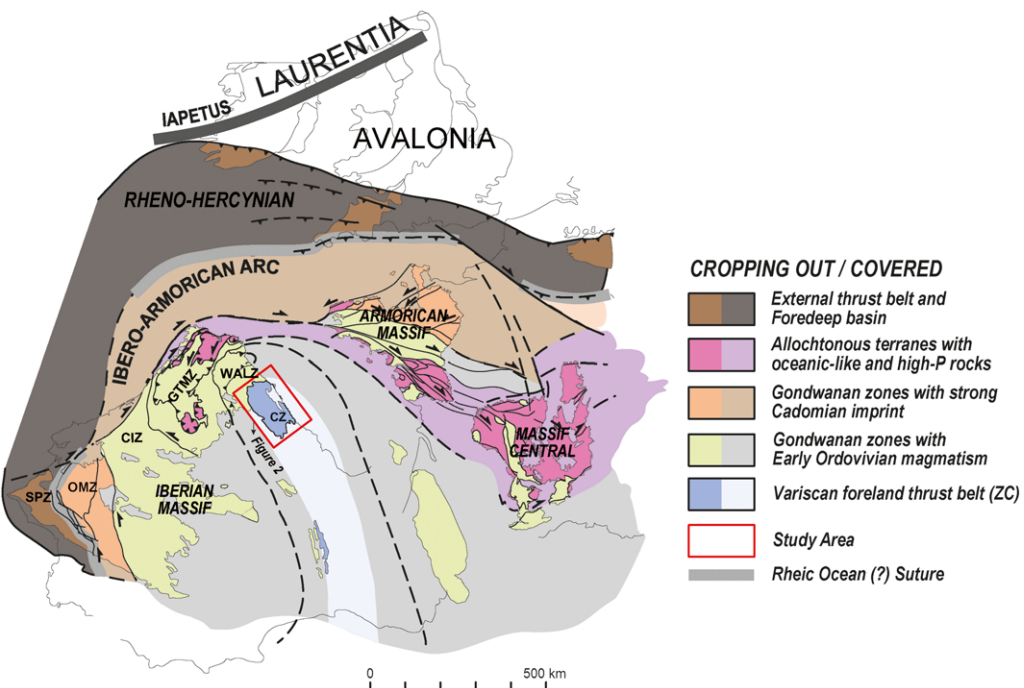
**Fig. 1.** Permian reconstruction of the West European Variscan Belt (according to Ballèvre *et al.* 2014, modified by Fernández-Lozano *et al.* 2016). The square indicates the location of the study area (Fig. 2); CZ, Cantabrian zone; WALZ, West Asturian Leonese zone; CIZ, Central Iberian zone, including part of the Galicia-Tras-os-Montes zone (GTMZ); OMZ, Ossa Morena zone; SPZ, South Portuguese zone.

Regional setting

The Variscan (Europe–NW Africa)–Alleghanian (North America) orogeny is a continental-scale tectonic system (1000 km wide and 8000 km long) that sutured Gondwana and Laurussia together, forming the supercontinent Pangaea (e.g. Domeier and Torsvik 2014; Edel *et al.* 2018; Pastor-Galán *et al.* 2019). This orogen formed as a consequence of a long tectonic history that involved several different tectonic events, from initial breakup of the Pannotia supercontinent giving rise to the Iapetus and Tornquist oceans to the subsequent Rheic ocean opening linked to the Avalonia undocking and finally to convergence (*c.* 420 Ma; e.g. Franke *et al.* 2017) leading to the amalgamation Gondwana and Laurussia into the latest supercontinent, Pangaea.

The Variscan–Alleghanian orogen itself represents the closing of at least one major ocean, the Rheic (e.g. Nance *et al.* 2010), whose axial ridge probably failed or was subducted at *c.* 395 Ma along its palaeonorthern margin (e.g. Woodcock *et al.* 2007; Gutiérrez-Alonso *et al.* 2008). There is no consensus whether the Variscan collision involved closure of several large oceans in addition to the Rheic (Stampfli *et al.* 2002; Franke *et al.* 2017, 2019) or several minor seaways and basins that existed between Gondwana and Laurussia, separated by several intervening microcontinents (e.g. Azor *et al.* 2008, Kroner and Romer 2013; Díez Fernández *et al.* 2016; Pérez-Cáceres *et al.* 2017). The onset of the Variscan orogeny, which led to the closure of all the oceans/basins, is interpreted to have been diachronous becoming progressively younger westwards (in present-day coordinates): with Devonian continent–continent collisions along the eastern boundary in the Bohemian Massif, progressing to earliest Permian ages in the westernmost sector in the Appalachians (e.g. Hatcher 2010; Franke *et al.* 2017).

Within this regional context, the Ediacaran to Permian geology of Iberia records, firstly, an Ediacaran Avalonian–Cadomian subduction environment with a thick siliciclastic and volcanic sequence intruded by igneous rocks, collectively interpreted to represent a back-arc basin (e.g. Fernández-Suárez *et al.* 1998; Murphy *et al.* 2004b, Linnemann *et al.* 2008; Pereira *et al.* 2012; Rubio-Ordóñez *et al.* 2015). The onset of the Paleozoic is characterized by rift-related igneous activity (Sánchez-García *et al.* 2008, 2019; Pereira *et al.* 2012) and the presence of a widespread angular unconformity that records deformation in the Ediacaran rocks which was not accompanied by cleavage development or metamorphism. The lower Paleozoic sequence collectively records the undocking of the Avalonian ribbon continent (Murphy *et al.* 2006; Nance *et al.* 2010) and the opening of the Rheic ocean in the early Ordovician,

which is attended by widespread rift-related igneous activity whose most important manifestation is the so-called 'Ollo de Sapo' event (e.g. Fernández-Suárez *et al.* 1999; Valverde-Vaquero and Dunning 2000; Murphy *et al.* 2008; Díez-Montes *et al.* 2010; Díez Fernández *et al.* 2012a). During the early Paleozoic, the Gondwanan margin in this region (the present-day Cantabrian Zone) recorded passive margin and rift-drift transition successions.

The passive margin preserves a complete Paleozoic sedimentary sequence consisting of alternating siliciclastic and carbonate formations in the proximal part of the shelf and dominantly siliciclastic formations in its distal oceanward regions (e.g. Gutiérrez-Marco *et al.* 2019). This passive margin was subjected to additional extension during the middle to late Ordovician (e.g. Clariana *et al.* 2018; Navidad *et al.* 2018) and in the early to middle Devonian transition, as revealed by facies changes and the local presence of rift-related volcanic rocks (Gutiérrez-Alonso *et al.* 2008).

The complete sedimentary sequence present in the Gondwana passive margin preserved in Iberia was deformed in the outermost shelf when the Rheic ocean closed, heralding the Variscan collision with Laurussia that eventually overrode the Gondwanan lower plate at *c.* 370 Ma (Santos Zalduegui *et al.* 1996; Rodríguez *et al.* 2003; López-Carmona *et al.* 2014; Arenas *et al.* 2014). During the Variscan orogeny the deformation propagated diachronously landwards, causing progressive shortening towards the northern Gondwana inner shelf spanning *c.* 50 Ma (Dallmeyer *et al.* 1997) and culminating with the orogenic extensional collapse that took place at *c.* 325–318 Ma (i.e. Rubio Pascual *et al.* 2013, López-Moro *et al.* 2018, Dias da Silva *et al.* 2020) in the hinterland. The extensional collapse slightly preceded or was coeval with the onset of the shortening in the foreland thrust-and-fold belt in the Cantabrian Zone (Figs 1 & 2).

Finally, the entire orogenic Variscan edifice in western Europe was buckled around a vertical axis leading to the formation of the Ibero-Armorican Orocline (IAO), especially evident in the Cantabrian Zone (Figs 1 & 2). Coeval folding and thrusting in the foreland fold and thrust belt, widespread magmatism and large topographic changes led to the generation of intramontane continental basins (e.g. Weil *et al.* 2019; Pastor-Galán *et al.* 2020 and references therein).

The Cantabrian Zone, compiled and new samples

The arcuate shaped Cantabrian Zone (herein CZ) of northern Iberia is situated in the core of the IAO (Gutiérrez-Alonso *et al.* 2004; Weil 2006;
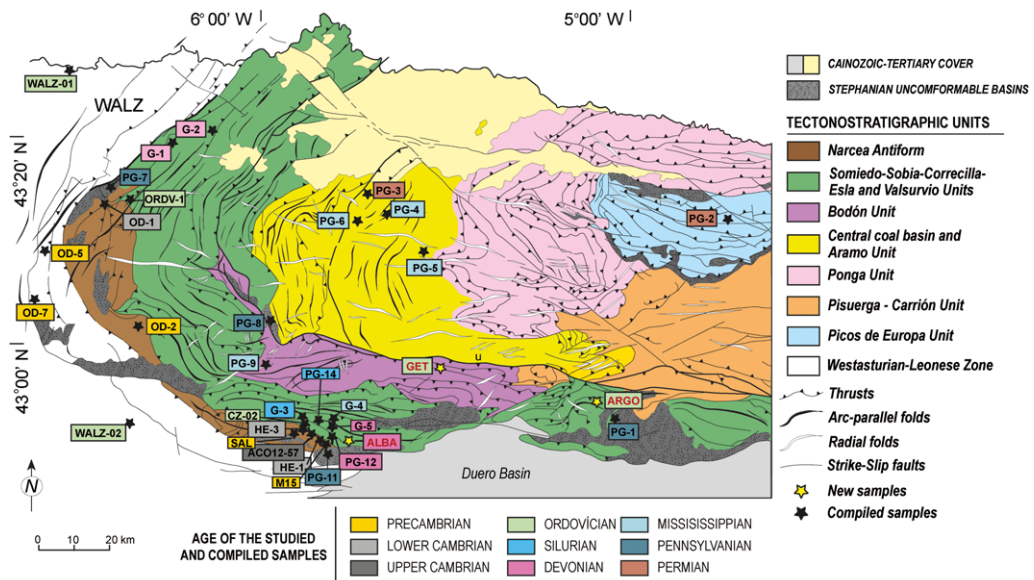
Fig. 2. Simplified structure/tectonic map of the Cantabrian Orocline from Alonso *et al.* (2009), showing the location of the samples used in this study.

Weil *et al.* 2019; Shaw *et al.* 2015) (Figs 1 & 2). The CZ is a classical foreland fold-and-thrust belt characterized by thin-skinned tectonics with a transport direction towards the core of the arc (Fig. 2; Julivert 1971, 1978; Pérez-Estaún *et al.* 1988; Alonso *et al.* 2009). The Variscan deformation in the CZ is late Mississippian to Pennsylvanian, diachronous towards the foreland, and resulted in the development of several clastic wedges related to the different thrust units (Marcos and Pulgar 1982). The first record of instability in the passive margin, owing to loading in the hinterland, is interpreted to have occurred in late Devonian times (Keller *et al.* 2008), but the sedimentary record of a fore-bulge and a fore-deep is not evident until the Mississipian (e.g. Agueda *et al.* 1991; Keller *et al.* 2007).

The CZ stratigraphic succession is very well constrained for the Paleozoic owing to its rich fossiliferous content. This succession begins with thick Neoproterozoic (Ediacaran) arc-related sequences (Fernández-Suárez *et al.* 2000; Rubio-Ordóñez *et al.* 2015), unconformably overlain by *c.* 4500 m of lower Paleozoic clastic and carbonate platformal strata (Fig. 2) that thin towards the east and culminate with a distinctive sequence of Silurian black shale and iron-rich sandstone (Fig. 2). Palaeocurrent data recorded in the lower Paleozoic strata indicate that its sediment source was located to the east in present day coordinates (Aramburu and García-Ramos 1993; Shaw *et al.* 2012), but there are no currently exposed potential source rocks. In the CZ, the

Devonian and Mississippian succession consists of alternating passive margin carbonate and siliciclastic formations (Fig. 3), which record multiple transgressive and regressive events (e.g. Aramburu and García-Ramos 1993; Keller *et al.* 2008; Merino-Tomé *et al.* 2017). This succession is conformably overlain by a *c.* 5000 m-thick Westphalian (Early–Middle Pennsylvanian; in this work we will use the West European Regional stages for the Pennsylvanian Carboniferous subsystem, which receives widespread use in the studied region) syn-orogenic sequence dominated by shallow marine and interbedded continental clastic strata (Marcos and Pulgar 1982; Merino-Tomé *et al.* 2017) followed by an unconformably overlying succession of Stephanian (upper Pennsylvanian) and early Permian age.

The Stephanian strata are younger westwards (e.g. Colmenero *et al.* 2002, 2008) and show little deformation. They are coal-bearing, continental, conglomerates, sandstones and shales (Figs 2 & 3) that show similar stratigraphic and sedimentological characteristics over much of northern Iberia. Permian continental red-beds and volcanics post-date the formation of the IAO (Weil *et al.* 2010; Pastor-Galán *et al.* 2011).

Within the stratigraphic record present in the CZ (Fig. 3) several previous detrital zircon studies have been performed, providing 26 statistically representative samples from the Cantabrian Zone and four more samples in the adjacent West Asturian–Leonese Zone (WALZ) (Fernández-Suárez *et al.* 2000,
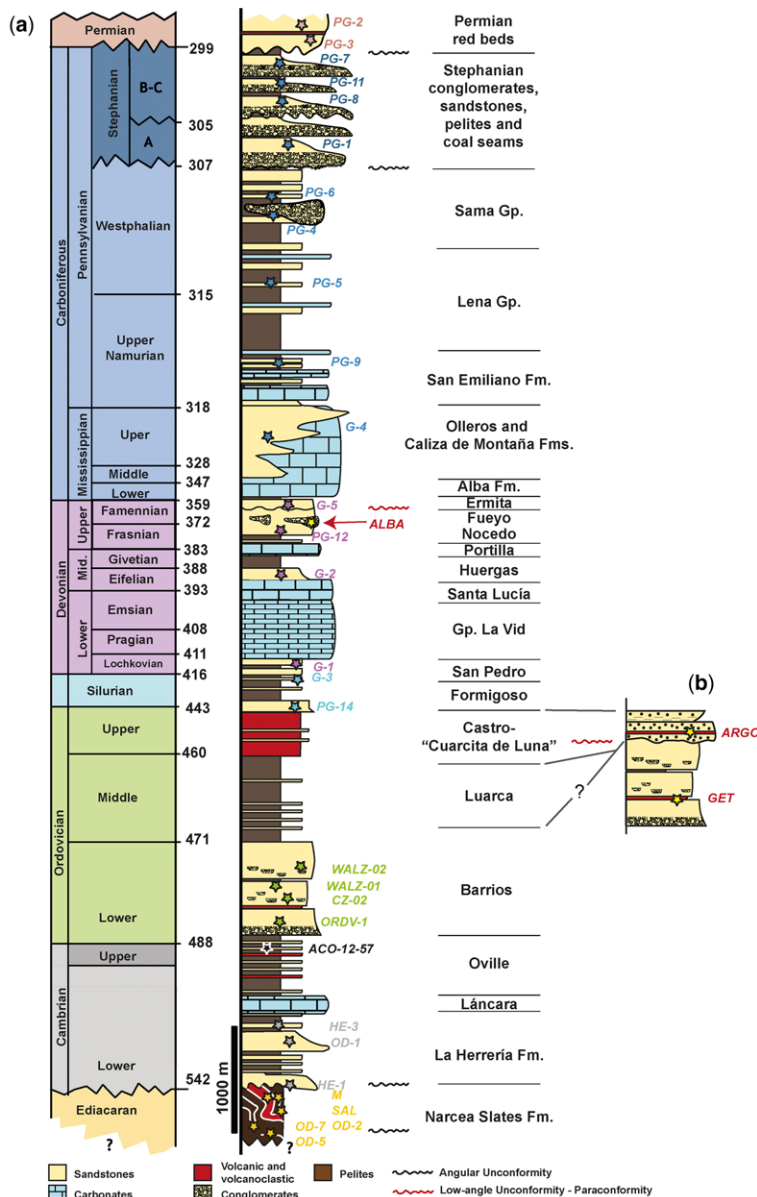
Fig. 3. Idealized stratigraphic column of the Cantabrian Zone showing the stratigraphic position of the new samples analysed in this study and the samples taken from the literature. (**a**) Synthetic stratigraphy of the Somiedo–Sobia–Correcilla–Esla and Valsurvio Units, including the Central coal basin in the western part of the Cantabrian Zone. (**b**) Ordovician local stratigraphy in the central part of the Cantabrian Zone. Stages for the Pennsylvanian subsystem are according to the Western European regional scale.

2002a, b, 2014; Gutiérrez-Alonso et al. 2003, 2015; Pastor-Galán et al. 2013a; Shaw et al. 2014; Zimmermann et al. 2015; Henderson et al. 2016; Naidoo et al. 2018). The Neoproterozoic samples (five) are from the Narcea Antiform (Figs 1 & 2; e.g. Gutiérrez-Alonso 1996; Shaw et al. 2015), an extensive Ediacaran outcrop of graywackes, slates and calc-alkaline igneous rocks. Samples OD-7 and OD-5 (Fernández-Suárez et al. 2014) correspond to the Allande Group (Rubio-Ordóñez et al. 2015), the oldest rocks exposed in the region. The other three samples (OD-2, SAL and M; Fernández-Suárez et al.

2014; Naidoo *et al.* 2018) are from the uppermost Ediacaran Navelgas Group (Rubio-Ordóñez *et al.* 2015) greywackes. Other previously studied Neoproterozoic samples from Fernández-Suárez *et al.* (2000, 2002*a*) and Gutiérrez-Alonso *et al.* (2003) were not included in our synthesis because of the paucity of data and their low statistical significance.

Four Cambrian samples (Fernández-Suárez *et al.* 2014; Zimmermann *et al.* 2015; Henderson *et al.* 2016) were collected in the Lower Cambrian Herrería Fm. (HE-1, OD-1 and HE-3) and in the Upper Cambrian Oville Fm. (ACO-12-57). Sample HE-1 was collected from the basal conglomerate of probable Tommotian age above the Ediacaran–Cambrian unconformity (Zimmermann *et al.* 2015). Samples OD-1 and H-3 were retrieved from the quartz-arenites of the middle and upper members, respectively, of the same Herrería Fm., both of Tommotian–Atdabanian age. Finally, sample ACO-12-57 (Henderson *et al.* 2016) corresponds to the uppermost part of the Oville Fm. quartzites of Guzhangian–Furongian age (Palacios 2015).

The detrital zircon U–Pb age populations of Ordovician rocks in the CZ were studied in four previously published samples (ORDV-1, CZ-2, WALZ-01 and WALZ-02; Fernández-Suárez *et al.* 2002*b*, Shaw *et al.* 2014). Two of the samples from Shaw *et al.* (2014) are from neighbouring areas of the WALZ and were used to enhance the consistency of the dataset as they were statistically identical to those in the CZ (Fig. 3). All of the mentioned samples were collected in the Armorican Quartzite (Barrios Fm. in the CZ and uppermost part of the Cabos Series in the WALZ). The samples are pure quartz-arenites and are part of the Armorican Quartzite facies that is a regional characteristic of the northern margin of Gondwana. The age of the samples is attributed to the Floian stage based on U–Pb dating of interbedded volcanic ash-fall deposits (477 Ma, U–Pb in zircon, Gutiérrez-Alonso *et al.* 2016).

The two Silurian samples from previously published works correspond to the Formigoso (sample PG14, Pastor-Galán *et al.* 2013*a*) and the lower part of the San Pedro (sample G-3, Gutiérrez-Alonso *et al.* 2015) formations. Both samples are sandstones. PG14 is interbedded with dark siltstones and lutites of Late Llandovery to Early Wenlock age and G-3 was collected at the base of a succession of intensely bioturbated ferruginous sandstones with rare ooid sandstones and local volcaniclastic beds of Ludlow age.

Four Devonian samples were used in this study (G-1, G-2, PG-12 and G5). Sample G-1 (Gutiérrez-Alonso *et al.* 2015) corresponds to the top of the previously described San Pedro Fm. and has a Lochkovian age. Sample G-2 (Gutiérrez-Alonso *et al.* 2015) was collected in the Naranco–Huergas Fm.,

composed of interbedded sandstones and shales of Eifelian to Early Givetian age. The samples from the Nocedo–Fueyo Fm. are G2 (Gutiérrez-Alonso *et al.* 2015) and PG-12 (Pastor-Galán *et al.* 2013*a*) and both were collected in sandstones interbedded with shales of Frasnian–Early Famenian age. Finally, sample G-5 (Gutiérrez-Alonso *et al.* 2015) corresponds to the Ermita Fm. consisting of quartzitic sandstones deposited across a low-angle regional unconformity, interpreted to represent the effects of the initial stages of the Variscan Orogeny (García-Ramos and Colmenero 1981; Rodríguez-Fernández *et al.* 1985; Keller *et al.* 2008). The depositional age of the Ermita Fm. is Upper Famenian.

The Carboniferous rocks in the CZ have a complex distribution in time and space (Colmenero *et al.* 2002) related to progressive Variscan tectonic activity. The nine compiled samples were collected in all sequences with siliciclastic rocks. Sample G-4 (Pastor-Galán *et al.* 2013*a*) corresponds to the first arrival of terrigenous debris from the developing orogenic belt, and was recovered from the turbiditic Olleros Fm. of Serpukhovian to early Bashkirian age. Sample PG-9 (Pastor-Galán *et al.* 2013*a*) is from the Bashkirian San Emiliano Fm. composed of turbiditic shales, sandstones and olitostromic limestones. Sample PG-5 (Pastor-Galán *et al.* 2013*a*) was collected in a paralic succession, the Sama Group, consisting of interbedded sandstone, shale and minor carbonate of upper Bashkirian to lower Moscovian age. Above these rocks, the Moscovian Lena Group is composed of shales, sandstones conglomerates, mineable coal seams and minor ash-fall beds. They are interpreted to have been deposited in proximal shelf and coastal environments (Merino-Tomé *et al.* 2017). Samples PG-4 and PG-6 (Pastor-Galán *et al.* 2013*a*) were taken from the base and the top of this unit, respectively. The last Carboniferous samples compiled (PG-1, PG-8, PG-11 and PG-7; Pastor-Galán *et al.* 2013*a*) correspond to conglomerate-rich continental sequences from various Stephanian (Kasimovian-Gzhelian) alluvial molassic basins unconformably overlying all the rocks in the region (Fig. 2).

Finally, the Permian samples (PG-3 and PG-2) are from basins dominated by continental red conglomerates, red shales and sandstones, with minor limestones, volcaniclastic rocks and calc-alkaline basaltic lava flows that were deposited in small basins (Martínez-García 1991) that post-date all of the Variscan deformation in the CZ (Weil *et al.* 2010; Pastor-Galán *et al.* 2011).

In order to complete the detrital zircon record, three new samples were collected and are presented in this paper. The new samples were collected in lower Ordovician recycled volcaniclastic rocks (sample GET: Figs 2 & 3), in upper Ordovician clastic rocks (sample ARGO: Figs 2 & 3) and in upper

Devonian conglomerates from the Fueyo formation (sample ALBA: Figs 2 & 3).

From bottom to top in the stratigraphic sequence the oldest of the new studied samples (GET; 42° 56'41.28″N 5°33'12.05″W) was collected in a volcaniclastic sequence with conglomeratic epiclastic tuffs, shales and greywackes within the lowermost part of the Barrios Fm., mostly of Floian age, where volcanic rocks are abundant, including tonstein type K bentonites (García-Ramos *et al.* 1984; Heinz *et al.* 1985; Gallastegui *et al.* 1992; Gutiérrez-Alonso *et al.* 2007, 2016). The analysed sample is a poorly sorted coarse-grained sandstone with abundant volcanic clasts. The volcanic clasts are rhyolitic tuffs partially replaced by zeolite and the remaining clasts are quartz and feldspar.

Sample ARGO (42°54'25.70″N 5°7'20.02″W) was collected in a decimetre-scale reworked ash layer in the upper part of a quarzitic sandstone bank formerly attributed to the Barrios Fm. and recently reassigned to the 'Cuarcita de Luna' (Gutiérrez-Marco *et al.* 2010; Bernárdez *et al.* 2014) or La Serrona Fm. (Toyos and Aramburu-Zabala 2014), attributed to glaciomarine sediments of Hirnantian age (Bernárdez *et al.* 2006; Gutiérrez-Marco *et al.* 2010; Fig. 3). Petrographically, it is a volcaniclastic siltstone with quartz and feldspar clasts in a hypoclastic matrix that also includes a significant amount of glass shards.

The third sample (ALBA, 42°48'17.86″N/5°43' 28.31″W) is a heterogeneous polymictic conglomerate containing pebbles of quartzite, chert, shale, carbonate and re-worked brachiopod fossils in a sandy matrix with carbonate cement. These conglomerates crop out discontinuously within the Fueyo Fm., which is Frasnian–Fammenian (Devonian) in age (Fig. 3).

This extensive dataset is used to test the detrital zircon populations' consistency in order to unravel the sources of sediments and sedimentary recycling owing to possible palaeogeographic changes or other tectonic events, including the role of mountain building processes during the Variscan orogeny.

Analytical methods

Twenty-nine zircon grains from sample GET, 51 from sample ARGO and 165 from sample ALBA were separated and extracted using the facilities at Salamanca University. Individual zircon grains were analysed for U, Th and Pb isotopes by LA–ICP–MS at the Museum für Mineralogie und Geologie (Senckenberg Naturhistorische Sammlungen Dresden), using a Thermo-Scientific Element 2 XR sector field ICP–MS coupled to a New Wave UP-193 Excimer Laser System. A teardrop-shaped, low-volume laser cell was used to enable sequential sampling of heterogeneous grains (e.g. growth zones) during time-resolved data acquisition. Each analysis consisted of 15 s background acquisition followed by 35 s data acquisition, using laser-spot sizes of 15–35 μm. A common-Pb correction based on the interference and background-corrected ^{204}Pb signal and a model Pb composition (Stacey and Kramers 1975) was carried out where necessary.

The criterion for correction was whether the corrected ^{207}Pb/^{206}Pb lay outside the internal error of measured ratios. Time-resolved signals of the LA–ICP–MS analyses were checked in order to detect disturbances caused by cracks or mineral inclusions. In such cases, analyses were excluded from age calculations. Raw data were corrected for background signals, common Pb, laser-induced elemental fractionation, instrumental mass discrimination and time-dependent elemental fractionation of Pb/Th and Pb/U using an Excel® spreadsheet program developed by A. Gerdes (Institute of Geosciences, Johann Wolfgang Goethe-University, Frankfurt am Main, Germany). Reported uncertainties were propagated by quadratic addition of the external reproducibility obtained from the standard zircon GJ-1 (*c.* 0.6 and 0.5–1% for the ^{207}Pb/^{206}Pb and ^{206}Pb/^{238}U, respectively) during individual analytical sessions and the within-run precision of each analysis. To calibrate the instrument GJ-1 standard analyses were repeated, giving ages of 607.8 $\pm$ 2.2 Ma (average age by ICP–MS of 608.5 $\pm$ 0.4 Ma; Jackson *et al.* 2004). The sequence of each analysis was six standards at first followed by 10 unknown zircon grains and three standards, repeating the two last sequences six times to complete in each cycle 60 analyses of unknown zircon grains and 23 standards (see Frei and Gerdes 2009 for further details).

Analyses with a concordance in the range 90–110% were used for concordia and probability density distribution plots. Discordance may originate from Pb loss, the addition of common Pb or ablation of different age domains within the zircon. Concordia diagrams (Figs 4, 5 & 6) were produced using Isoplot/Ex 3.7 (Ludwig 2001). For concordant analyses (i.e. analyses whose 2σ error ellipse intercepts the concordia curve) we used concordia ages and errors (Ludwig 1998) as calculated by Isoplot. For discordant analyses (still within the 90–110% concordance range) older than 1000 Ma we use the more precise ^{207}Pb/^{206}Pb age. Further details on analytical protocol and data processing may be found in Frei and Gerdes (2009).

Results

The results obtained in the studied samples are listed in Table 1 and shown in Figures 4–6 through
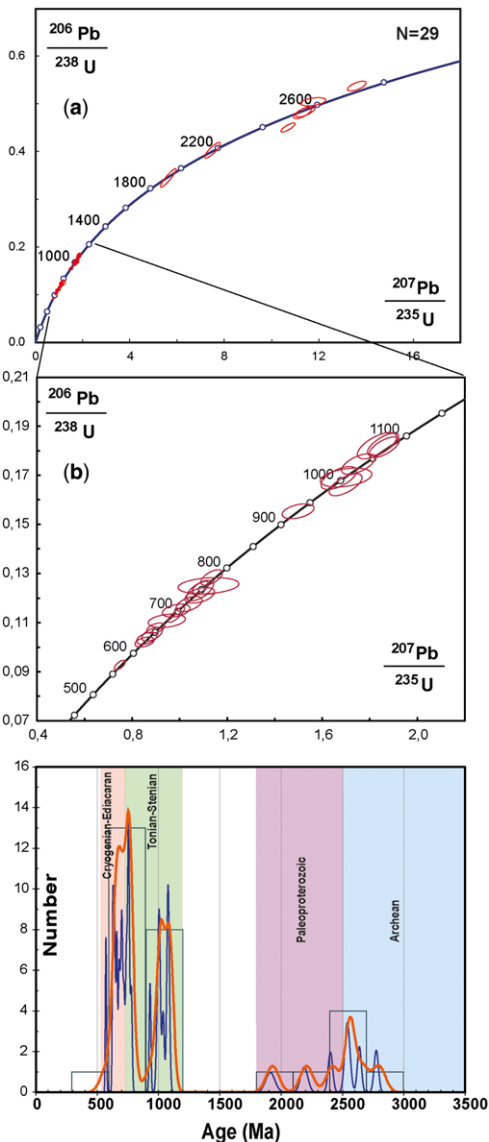
Fig. 4. Concordia diagrams showing the U–Pb results of the analyses performed on sample GET. (a) complete dataset, (b) detail of the ages between 500 and 1200 Ma. Probability density plot (blue), KDE (orange) and histogram of the detrital zircon ages found in this sample.

Fig. 5. Concordia diagrams showing the U–Pb results of the analyses performed on sample ARGO. (a) complete dataset, (b) detail of the ages between 400 and 1200 Ma. Probability density plot (blue), KDE (orange) and histogram of the detrital zircon ages found in this sample.

concordia diagrams, PDPs and KDEs, respectively. The 29 concordant ($\pm 10\%$ of concordance, Table 1) zircon grains in sample GET (Figs 2 & 3) show an age spectrum from 571 ± 10 to 2775 ± 36 Ma (Fig. 4a, b) and are concentrated mostly between 570 and 1100 Ma. Three maxima can be observed in the PDPs (Fig. 4c) that are coincident

with zircon ages that correspond to (1) zircon grains derived from the igneous activity during the Avalonian–Cadomian cycle, between 540 and 800 Ma, (2) zircon grains with ages from 950 to 1100 Ma (Tonian–Stenian) attributed to the amalgamation of Rodinia (Grenville orogeny, Condie and Aster 2010) and minor peaks with (3) Paleoproterozoic
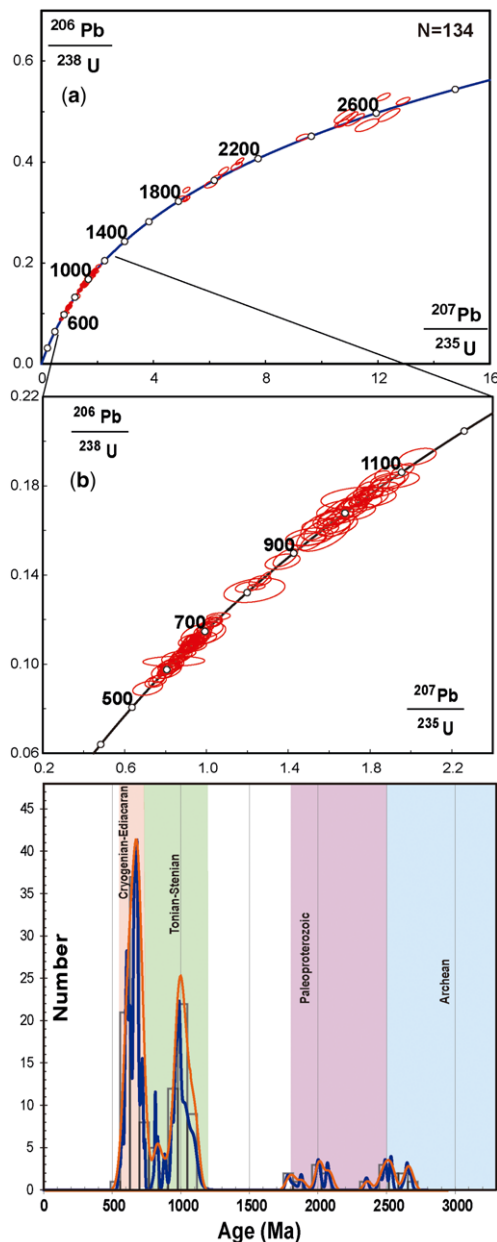
Fig. 6. Concordia diagrams showing the U–Pb results of the analyses performed on sample ALBA. (a) complete dataset, (b) detail of the ages between 500 and 1200 Ma. Probability density plot (blue), KDE (orange) and histogram of the detrital zircon ages found in this sample.

(c. 1.8–2.2 Ga) and (4) Archaean (c. 2.5–3.3 Ga) ages. No zircon grains of Paleozoic age coeval with the putative age of the volcanic component of this sample have been found.

Sample ARGO (Figs 2 & 3) provided 51 zircon grains which yielded concordant ages between 492 ± 10 and 2720 ± 66 Ma, shown in Table 1 and Figure 5. The four maxima (Fig. 5c) are coincident with those described in sample GET except for the appearance of the Tonian–Stenian population, which is larger in sample ARGO. In addition, this sample provided a zircon with a Furgonian (492 ± 10 Ma, latest Cambrian) age which, given the stratigraphic position of the sample, is also considered a reworked grain.

Despite the paucity of zircon grains recovered from the two aforementioned samples and their possible lack of statistical robustness, the results obtained are coherent with data from other samples of similar ages and locations. Thus, we consider them significant and usable in the compilation presented in this work.

Sample ALBA (Figs 2 & 3) provided 134 concordant ages (Table 1, Fig. 6) ranging from 551 to 2531 Ma. The obtained ages cluster in the same intervals as the previously described samples, the group with Ediacaran–Cryogenian ages being the most abundant.

Sample comparison: multidimensional scaling

Results from the new samples were integrated into the existing zircon age dataset in the region (30 samples, 3764 U–Pb zircon ages) and compared visually using their KDEs through time (Fig. 7). All of the KDE plots show similar dominant age groups (maxima): Ediacaran–Cryogenian (c. 0.55–0.8 Ga), Tonian–Stenian (c. 0.85–1.2 Ga), Paleoproterozoic (c. 1.8–2.2 Ga) and Archaean (c. 2.5–3.3 Ga). Some of the samples are lacking some of the peaks (see the lower Cambrian samples, especially OD-1 and HE-3, which are the only ones completely lacking the Tonian–Stenian population) and the relative abundances of the different populations also reveal variations through time. These variations in the KDE functions are not straightforward to interpret, nor is it easy to establish their similarity/dissimilarity in a quantitative way. It is also difficult to describe the role of zircon recycling from underlying sedimentary rocks and/or to interpret similarities or differences when samples are far apart in time. On the other hand, KDEs are very useful for identifying the appearance of new populations that reveal the presence of new sources of zircon in the studied region (Fig. 7, note the changes with new age populations in samples G-4 and PG-5).

In order to perform a more robust comparison of the samples, cumulative age distributions (CADs) can also be used. CADs reveal the similarities/dissimilarities within a set of samples as the degree of

G. Gutiérrez-Alonso et al.

Table 1. *LA–ICP–MS U–Pb results*

Analysis no.	Isotopic ratios and 2σ (%) errors							Ages and 2σ absolute errors (Ma)						Concordance (%)*
	$^{206}Pb/^{238}U$	$\pm 2\sigma$	$^{207}Pb/^{235}U$	$\pm 2\sigma$	$^{207}Pb/^{206}Pb$	$\pm 2\sigma$	ρ	$^{206}Pb/^{238}U$	$\pm 2\sigma$	$^{207}Pb/^{235}U$	$\pm 2\sigma$	$^{207}Pb/^{206}Pb$	$\pm 2\sigma$	
GET														
a45	0.0927	1.77	0.7488	2.60	0.0586	1.90	0.679761	571	10	568	11	552	42	103.5
a46	0.1021	1.60	0.8534	3.90	0.0606	3.55	0.411040	627	10	626	18	626	77	100.2
a48	0.1037	1.92	0.8626	4.16	0.0603	3.69	0.461878	636	12	632	20	616	80	103.3
a33	0.1053	2.16	0.8843	3.95	0.0609	3.31	0.546091	645	13	643	19	636	71	101.4
a60	0.1078	1.60	0.8999	3.47	0.0605	3.07	0.462586	660	10	652	17	622	66	106.1
a38	0.1108	2.02	0.9461	6.80	0.0619	6.50	0.296700	677	13	676	34	672	139	100.8
a34	0.1134	2.30	0.9873	2.81	0.0632	1.62	0.817748	692	15	697	14	714	34	97.0
a56	0.1150	1.83	0.9853	4.89	0.0621	4.53	0.374402	702	12	696	25	678	97	103.5
a44	0.1177	2.19	1.0404	4.31	0.0641	3.71	0.508512	717	15	724	23	746	78	96.2
a37	0.1211	2.11	1.0840	4.64	0.0649	4.14	0.454164	737	15	746	25	772	87	95.5
a58	0.1230	2.67	1.0865	4.21	0.0640	3.25	0.634790	748	19	747	22	743	69	100.7
a42	0.1243	1.60	1.0881	2.63	0.0635	2.09	0.608398	755	11	748	14	725	44	104.2
a53	0.1250	2.11	1.1215	9.25	0.0651	9.01	0.228296	759	15	764	51	777	189	97.6
a52	0.1283	2.01	1.1339	3.32	0.0641	2.64	0.605865	778	15	770	18	745	56	104.4
a36	0.1553	1.57	1.4980	3.67	0.0699	3.32	0.428196	931	14	930	23	927	68	100.4
a31	0.1662	2.17	1.6973	3.33	0.0741	2.52	0.653644	991	20	1008	21	1044	51	94.9
a41	0.1689	2.23	1.6690	3.68	0.0717	2.93	0.605721	1006	21	997	24	976	60	103.1
a50	0.1690	1.87	1.6991	5.23	0.0729	4.89	0.356795	1007	17	1008	34	1011	99	99.6
a59	0.1746	1.96	1.7505	3.30	0.0727	2.66	0.591983	1037	19	1027	22	1006	54	103.1
a39	0.1814	1.89	1.8589	2.83	0.0743	2.12	0.665068	1075	19	1067	19	1050	43	102.4
a40	0.1821	2.40	1.8299	3.68	0.0729	2.79	0.652602	1078	24	1056	24	1011	57	106.7
a32	0.1826	2.02	1.8541	2.85	0.0736	2.00	0.710910	1081	20	1065	19	1031	40	104.8
a35	0.3451	4.55	5.6307	4.94	0.1183	1.93	0.920279	1911	76	1921	44	1931	35	99.0
a51	0.4040	3.19	7.4785	3.69	0.1342	1.86	0.863676	2188	59	2170	34	2154	32	101.5
a43	0.4514	1.85	10.6992	2.29	0.1719	1.34	0.810072	2401	37	2497	21	2576	22	93.2
a55	0.4816	1.90	11.3323	2.71	0.1707	1.94	0.699868	2534	40	2551	26	2564	32	98.8
a54	0.4843	2.01	11.4413	2.86	0.1713	2.04	0.703197	2546	42	2560	27	2571	34	99.0
a49	0.5055	1.51	11.7748	3.70	0.1689	3.38	0.407509	2638	33	2587	35	2547	57	103.6
a57	0.5380	1.57	13.6217	2.40	0.1836	1.81	0.656788	2775	36	2724	23	2686	30	103.3
ARGO														
a16	0.0793	2.01	0.6244	4.80916836	0.0571	4.37	0.418721	492	10	493	19	497	96	99.0
a7	0.0924	1.26	0.7442	3.764726198	0.0584	3.55	0.333796	569	7	565	16	546	78	104.3
a39	0.1022	1.80	0.8488	3.378989869	0.0602	2.86	0.533446	627	11	624	16	612	62	102.4
a35	0.1023	1.88	0.8637	3.238878005	0.0612	2.64	0.580099	628	11	632	15	646	57	97.2

a28	0.1049	1.57	0.8788	2.856536219	0.0608	2.39	0.549953	643	10	640	14	631	51	101.8
a29	0.1054	1.86	0.8802	3.133646358	0.0606	2.52	0.594927	646	11	641	15	624	54	103.4
a57	0.1070	1.40	0.8998	4.592909154	0.0610	4.37	0.304988	655	9	652	22	640	94	102.4
a32	0.1076	1.18	0.9251	2.158131712	0.0623	1.81	0.545533	659	7	665	11	686	39	96.1
a34	0.1101	2.05	0.9506	12.54436898	0.0626	12.38	0.163444	673	13	678	64	696	264	96.7
a60	0.1115	1.00	0.9707	2.99569115	0.0631	2.82	0.333241	682	6	689	15	712	60	95.7
a41	0.1122	1.86	0.9656	4.062859433	0.0624	3.61	0.457946	686	12	686	20	688	77	99.7
a10	0.1143	1.93	1.0048	3.631542759	0.0638	3.07	0.532175	698	13	706	19	734	65	95.1
a15	0.1154	1.42	0.9850	3.137747523	0.0619	2.80	0.454130	704	10	696	16	671	60	104.9
a51	0.1164	1.86	1.0231	2.817820197	0.0637	2.12	0.659181	710	12	715	15	733	45	96.9
a43	0.1165	2.68	1.0239	5.515573437	0.0638	4.82	0.485164	710	18	716	29	734	102	96.8
a59	0.1198	1.02	1.0481	5.140785067	0.0634	5.04	0.197796	730	7	728	27	723	107	101.0
a24	0.1213	1.48	1.0724	3.373348295	0.0641	3.03	0.438497	738	10	740	18	746	64	99.0
a30	0.1222	1.84	1.0986	2.945452995	0.0652	2.30	0.624581	743	13	753	16	781	48	95.1
a11	0.1277	1.86	1.1622	2.808505266	0.0660	2.11	0.661647	775	14	783	15	807	44	96.0
a4	0.1298	1.04	1.1745	2.378588491	0.0656	2.14	0.437895	787	8	789	13	794	45	99.0
a21	0.1352	1.59	1.2506	3.043731068	0.0671	2.60	0.522120	817	12	824	17	841	54	97.2
a55	0.1511	1.79	1.4402	2.855374519	0.0691	2.22	0.627421	907	15	906	17	902	46	100.6
a27	0.1522	1.41	1.4564	2.599174057	0.0694	2.19	0.540955	914	12	913	16	910	45	100.4
a3	0.1570	1.61	1.5455	2.513853852	0.0714	1.93	0.641015	940	14	949	16	968	39	97.1
a48	0.1629	1.81	1.5628	5.019118692	0.0696	4.68	0.360586	973	16	956	32	917	96	106.1
a12	0.1631	1.49	1.6375	3.2746191	0.0728	2.91	0.456150	974	14	985	21	1009	59	96.5
a5	0.1652	2.18	1.6665	16.55629519	0.0732	16.41	0.131910	985	20	996	111	1019	332	96.7
a56	0.1699	1.21	1.7500	2.054061103	0.0747	1.66	0.588800	1012	11	1027	13	1060	33	95.4
a17	0.1711	2.01	1.7078	3.525441759	0.0724	2.90	0.569139	1018	19	1011	23	997	59	102.1
a44	0.1723	1.11	1.7278	2.726587036	0.0727	2.49	0.408729	1025	11	1019	18	1007	50	101.8
a18	0.1731	1.58	1.7657	2.582589797	0.0740	2.04	0.613230	1029	15	1033	17	1041	41	98.8
a33	0.1743	1.58	1.7694	3.772366356	0.0736	3.43	0.418346	1036	15	1034	25	1032	69	100.4
a25	0.1754	1.42	1.8270	2.616638276	0.0756	2.20	0.542879	1042	14	1055	17	1083	44	96.1
a53	0.1763	1.67	1.7474	2.518547704	0.0719	1.89	0.662920	1047	16	1026	16	983	38	106.5
a42	0.1779	1.29	1.8276	3.942151199	0.0745	3.72	0.327556	1055	13	1055	26	1055	75	100.0
a38	0.1786	2.09	1.7973	4.254857723	0.0730	3.71	0.491197	1059	20	1044	28	1014	75	104.5
a50	0.1788	1.62	1.8262	2.415655268	0.0741	1.79	0.669982	1061	16	1055	16	1043	36	101.7
a8	0.1824	1.39	1.8315	3.037760425	0.0728	2.70	0.458827	1080	14	1057	20	1009	55	107.1
a58	0.1866	1.71	1.9778	4.015992288	0.0769	3.63	0.426493	1103	17	1108	27	1118	72	98.7
a40	0.3104	1.45	4.7588	2.144118536	0.1112	1.58	0.674829	1743	22	1778	18	1819	29	95.8
a22	0.3244	1.30	4.8253	2.097965585	0.1079	1.65	0.618637	1811	21	1789	18	1764	30	102.7
a54	0.3463	2.05	5.6848	2.653436064	0.1191	1.68	0.773917	1917	34	1929	23	1942	30	98.7
a13	0.3495	1.92	5.7055	2.607904874	0.1184	1.76	0.736505	1932	32	1932	23	1932	32	100.0
a46	0.3552	1.56	5.6964	2.231498249	0.1163	1.60	0.698640	1959	26	1931	19	1901	29	103.1
a45	0.3728	1.29	6.0295	2.693045045	0.1173	2.36	0.479434	2043	23	1980	24	1915	42	106.7

Table 1. *LA–ICP–MS U–Pb results* (*Continued*)

Analysis no.	Isotopic ratios and 2σ (%) errors							Ages and 2σ absolute errors (Ma)						Concordance (%)*
	$^{206}Pb/^{238}U$	$\pm2\sigma$	$^{207}Pb/^{235}U$	$\pm2\sigma$	$^{207}Pb/^{206}Pb$	$\pm2\sigma$	ρ	$^{206}Pb/^{238}U$	$\pm2\sigma$	$^{207}Pb/^{235}U$	$\pm2\sigma$	$^{207}Pb/^{206}Pb$	$\pm2\sigma$	
a52	0.3782	3.98	6.8451	5.248531791	0.1313	3.42	0.757990	2068	71	2092	48	2115	60	97.8
a47	0.3792	1.48	6.9444	2.005490904	0.1328	1.35	0.739015	2073	26	2104	18	2135	24	97.1
a19	0.4560	1.47	9.5361	1.854374177	0.1517	1.13	0.791652	2422	30	2391	17	2365	19	102.4
a6	0.4798	1.38	10.9620	1.847114118	0.1657	1.22	0.749041	2526	29	2520	17	2515	21	100.5
a20	0.5197	1.23	12.2378	1.454746136	0.1708	0.78	0.845872	2698	27	2623	14	2565	13	105.2
a49	0.5250	2.97	12.9201	3.389674791	0.1785	1.63	0.876714	2720	66	2674	32	2639	27	103.1
ALBA														
c2	0.08925066	2.96834215	0.7129	8.382883163	0.0579	7.84	0.354096	551	16	546	36	527	172	105
b37	0.09228612	2.38519372	0.7519	5.707859007	0.0591	5.19	0.417879	569	13	569	25	570	113	100
c20	0.09279302	2.30501434	0.7571	4.300816879	0.0592	3.63	0.535948	572	13	572	19	574	79	100
c12	0.09375893	1.77473516	0.7691	3.522613571	0.0595	3.04	0.503812	578	10	579	16	585	66	99
c48	0.09603505	1.90813725	0.8021	4.119545644	0.0606	3.65	0.463191	591	11	598	19	624	79	95
b2	0.09682090	1.50780264	0.8101	2.673336832	0.0607	2.21	0.564015	596	9	602	12	628	48	95
b54	0.09716681	3.07116309	0.8045	7.429644536	0.0600	6.77	0.413366	598	18	599	34	605	146	99
a1	0.09716883	2.26973016	0.7912	3.38348045	0.0591	2.51	0.670827	598	13	592	15	569	55	105
b31	0.09804444	2.31247190	0.8225	4.657741191	0.0608	4.04	0.496479	603	13	609	22	634	87	95
b59	0.09815505	1.89845662	0.8183	4.700326131	0.0605	4.30	0.403899	604	11	607	22	620	93	97
b35	0.09826746	2.07141926	0.8165	3.661520453	0.0603	3.02	0.565727	604	12	606	17	613	65	99
c42	0.09848538	2.54534789	0.8218	5.097966458	0.0605	4.42	0.499287	606	15	609	24	622	95	97
b27	0.09890142	1.40676190	0.8206	4.781160056	0.0602	4.57	0.294230	608	8	608	22	610	99	100
c15	0.09929019	2.08550912	0.8213	5.878891564	0.0600	5.50	0.354745	610	12	609	27	603	119	101
b24	0.09934565	2.74697712	0.8272	6.186933795	0.0604	5.54	0.443997	611	16	612	29	618	120	99
c5	0.09959331	2.13925689	0.8298	3.682349904	0.0604	3.00	0.580949	612	13	614	17	619	65	99
c27	0.10032388	2.59164073	0.8487	3.448463518	0.0614	2.27	0.751535	616	15	624	16	652	49	95
c4	0.10039509	1.45725795	0.8381	2.614991586	0.0605	2.17	0.557271	617	9	618	12	623	47	99
a28	0.10130566	1.79640696	0.8403	14.7023521	0.0602	14.59	0.122185	622	11	619	71	609	315	102
c14	0.10174999	2.02149947	0.8568	3.497254816	0.0611	2.85	0.578025	625	12	628	17	642	61	97
a24	0.10231758	1.58716133	0.8694	2.654632761	0.0616	2.13	0.597884	628	10	635	13	661	46	95
b25	0.10250129	2.06237118	0.8613	4.319690259	0.0609	3.80	0.477435	629	12	631	21	637	82	99
c10	0.10290625	1.87006945	0.8549	3.44932218	0.0603	2.90	0.542156	631	11	627	16	613	63	103
c7	0.10291374	2.23505865	0.8480	6.466073245	0.0598	6.07	0.345659	631	13	624	31	595	131	106
c21	0.10378378	2.40002144	0.8816	4.549075628	0.0616	3.86	0.527584	637	15	642	22	661	83	96
a3	0.10417508	2.17382460	0.8622	3.445724913	0.0600	2.67	0.630876	639	13	631	16	604	58	106
b55	0.10470240	1.31694731	0.8976	4.567764335	0.0622	4.37	0.288313	642	8	650	22	680	93	94
a18	0.10632455	2.09445070	0.8858	2.933549762	0.0604	2.05	0.713965	651	13	644	14	619	44	105
c60	0.10700257	1.58369890	0.9027	3.658366411	0.0612	3.30	0.432898	655	10	653	18	646	71	101

G. Gutiérrez-Alonso *et al.*

c34	0.10704234	2.31579974	0.9055	3.806119659	0.0614	3.02	0.608441	656	14	655	19	652	65	101
c58	0.10709753	1.79175921	0.9101	3.523293636	0.0616	3.03	0.508547	656	11	657	17	661	65	99
b14	0.10715843	1.76825383	0.9199	3.164141305	0.0623	2.62	0.558842	656	11	662	16	683	56	96
c13	0.10765789	2.42102525	0.9233	3.897455298	0.0622	3.05	0.621181	659	15	664	19	681	65	97
b22	0.10799706	1.79640962	0.9356	5.641842521	0.0628	5.35	0.318408	661	11	671	28	702	114	94
c17	0.10810594	2.33544419	0.9247	3.324494347	0.0620	2.37	0.702496	662	15	665	16	675	51	98
a15	0.10816606	1.82469518	0.9352	3.757496273	0.0627	3.28	0.485615	662	11	670	19	698	70	95
b45	0.10851649	1.95523079	0.9239	3.002640953	0.0617	2.28	0.651170	664	12	664	15	665	49	100
a16	0.10867060	2.00987949	0.9413	4.435112037	0.0628	3.95	0.453174	665	13	674	22	702	84	95
b51	0.10884738	1.89035427	0.9344	5.017776819	0.0623	4.65	0.376731	666	12	670	25	683	99	97
b3	0.10925636	1.96577351	0.9282	3.541036814	0.0616	2.95	0.555141	668	12	667	17	661	63	101
c43	0.10966041	1.41181507	0.9388	3.812163561	0.0621	3.54	0.370345	671	9	672	19	677	76	99
b58	0.10978966	2.00270588	0.9385	3.926864614	0.0620	3.38	0.510001	672	13	672	19	674	72	100
b48	0.10981243	1.44576693	0.9414	3.472691014	0.0622	3.16	0.416325	672	9	674	17	680	67	99
b46	0.10984295	2.78524396	0.9234	4.542461382	0.0610	3.59	0.613157	672	18	664	22	638	77	105
b1	0.10990679	1.56874750	0.9413	3.361724523	0.0621	2.97	0.466650	672	10	674	17	678	64	99
b13	0.11056732	2.31441472	0.9348	6.288847199	0.0613	5.85	0.368019	676	15	670	31	651	126	104
a5	0.11075253	2.08708909	0.9505	3.427349562	0.0622	2.72	0.608951	677	13	678	17	683	58	99
c33	0.11123500	1.33678816	0.9513	2.273913802	0.0620	1.84	0.587880	680	9	679	11	675	39	101
c28	0.11134847	1.56337242	0.9476	4.806022918	0.0617	4.54	0.325294	681	10	677	24	665	97	102
c59	0.11140286	1.15785782	0.9532	4.700561676	0.0621	4.56	0.246323	681	7	680	24	676	97	101
c40	0.11165467	2.02279885	0.9765	6.162104338	0.0634	5.82	0.328264	682	13	692	31	723	123	94
c49	0.11194616	1.74593769	0.9396	2.31735136	0.0609	1.52	0.753419	684	11	673	11	635	33	108
b52	0.11203471	2.31100554	0.9704	4.409700375	0.0628	3.76	0.524073	685	15	689	22	702	80	98
b33	0.11206519	1.89251856	0.9659	3.57192132	0.0625	3.03	0.529832	685	12	686	18	692	65	99
c53	0.11251990	1.29904717	0.9645	2.563478673	0.0622	2.21	0.506752	687	8	686	13	680	47	101
b20	0.11262306	2.41764661	0.9907	2.941236938	0.0638	1.68	0.821983	688	16	699	15	735	35	94
c55	0.11280703	2.06126933	0.9758	3.513377958	0.0627	2.85	0.586692	689	13	691	18	699	61	99
a25	0.11362377	3.66785686	0.9849	9.051313498	0.0629	8.27	0.405229	694	24	696	47	704	176	99
c38	0.11410322	1.66584877	0.9805	3.10671094	0.0623	2.62	0.536210	697	11	694	16	685	56	102
c24	0.11522782	2.48026215	1.0099	5.774503581	0.0636	5.21	0.429520	703	17	709	30	727	111	97
a27	0.11625353	1.20091864	1.0040	2.610779603	0.0626	2.32	0.459985	709	8	706	13	696	49	102
a9	0.11644422	2.10424155	0.9873	2.958536869	0.0615	2.08	0.711244	710	14	697	15	657	45	108
c51	0.11781991	0.92521210	1.0153	3.87485041	0.0625	3.76	0.238774	718	6	712	20	691	80	104
a30	0.11877106	1.59860448	1.0291	3.976617924	0.0628	3.64	0.402001	723	11	718	21	703	78	103
c47	0.11879851	1.27803602	1.0348	3.100313242	0.0632	2.82	0.412228	724	9	721	16	714	60	101
a23	0.11911679	2.05062702	1.0277	3.751431749	0.0626	3.14	0.546625	725	14	718	19	694	67	105
b8	0.12137629	1.10590349	1.0590	4.441738664	0.0633	4.30	0.248980	738	8	733	23	718	91	103
c25	0.13311790	3.33622240	1.2346	9.880029847	0.0673	9.30	0.337673	806	25	816	57	846	193	95
c9	0.13460685	1.39875590	1.1980	3.873051156	0.0646	3.61	0.361151	814	11	800	22	760	76	107
b23	0.13477290	0.83539735	1.2446	2.816414756	0.0670	2.69	0.296617	815	6	821	16	837	56	97

(*Continued*)

Table 1. *LA–ICP–MS U–Pb results* (*Continued*)

Analysis no.	Isotopic ratios and 2σ (%) errors							Ages and 2σ absolute errors (Ma)						Concordance (%)*
	^{206}Pb/^{238}U	$\pm 2\sigma$	^{207}Pb/^{235}U	$\pm 2\sigma$	^{207}Pb/^{206}Pb	$\pm 2\sigma$	ρ	^{206}Pb/^{238}U	$\pm 2\sigma$	^{207}Pb/^{235}U	$\pm 2\sigma$	^{207}Pb/^{206}Pb	$\pm 2\sigma$	
b57	0.13736201	1.42118199	1.2618	3.541965802	0.0666	3.24	0.401241	830	11	829	20	826	68	100
c45	0.13829020	1.84138714	1.2794	2.232167213	0.0671	1.26	0.824932	835	14	837	13	841	26	99
a6	0.14596689	1.95027464	1.3722	5.081003752	0.0682	4.69	0.383836	878	16	877	30	874	97	100
a8	0.14775597	2.24830866	1.3859	3.539805801	0.0680	2.73	0.635150	888	19	883	21	869	57	102
b17	0.15539992	2.27027729	1.5220	3.379223559	0.0710	2.50	0.671834	931	20	939	21	958	51	97
c37	0.15603027	1.45048189	1.4965	4.904550555	0.0696	4.69	0.295742	935	13	929	30	915	96	102
b5	0.15708324	2.11171646	1.5034	6.339701314	0.0694	5.98	0.333094	941	19	932	39	911	123	103
c3	0.15839116	3.98958425	1.5721	6.814111177	0.0720	5.52	0.585489	948	35	959	43	986	112	96
a26	0.16019152	1.20116424	1.5969	2.544560974	0.0723	2.24	0.472052	958	11	969	16	994	46	96
a20	0.16024728	2.36566579	1.5476	3.791388338	0.0700	2.96	0.623958	958	21	950	24	930	61	103
c26	0.16202098	1.65897878	1.6344	3.45139527	0.0732	3.03	0.480669	968	15	984	22	1018	61	95
b29	0.16205219	2.35534719	1.6387	5.000619137	0.0733	4.41	0.471011	968	21	985	32	1023	89	95
b41	0.16233298	3.56383612	1.5921	6.723404593	0.0711	5.70	0.530064	970	32	967	43	961	116	101
a13	0.16234348	1.46689232	1.5592	4.837409764	0.0697	4.61	0.303239	970	13	954	30	918	95	106
b34	0.16485517	1.34826622	1.6263	2.788408374	0.0715	2.44	0.483525	984	12	980	18	973	50	101
b42	0.16504675	2.07194335	1.6093	4.475947261	0.0707	3.97	0.462906	985	19	974	28	949	81	104
c52	0.16533954	1.55882108	1.6001	2.918732268	0.0702	2.47	0.534075	986	14	970	18	934	51	106
b40	0.16645225	1.92603416	1.6559	3.292275262	0.0721	2.67	0.585016	993	18	992	21	990	54	100
b32	0.16661679	2.00391325	1.6350	4.195445502	0.0712	3.69	0.477640	993	18	984	27	962	75	103
c11	0.16692018	1.82060198	1.6886	3.210635627	0.0734	2.64	0.567053	995	17	1004	21	1024	54	97
b60	0.16754351	3.35651062	1.6264	4.306386761	0.0704	2.70	0.779426	999	31	980	27	940	55	106
b9	0.16835466	1.75478167	1.7416	4.001410962	0.0750	3.60	0.438541	1003	16	1024	26	1069	72	94
c36	0.16917966	2.14949370	1.6622	6.078698187	0.0713	5.69	0.353611	1008	20	994	39	965	116	104
c16	0.17087402	2.47622155	1.7116	4.154145468	0.0726	3.34	0.596084	1017	23	1013	27	1004	68	101
c46	0.17143906	1.53074972	1.7160	3.355293618	0.0726	2.99	0.456219	1020	14	1015	22	1003	61	102
b15	0.17223155	1.82333047	1.7628	4.355005243	0.0742	3.95	0.418675	1024	17	1032	29	1048	80	98
c30	0.17263186	1.21681197	1.7005	1.986333389	0.0714	1.57	0.612592	1027	12	1009	13	970	32	106
c56	0.17332876	1.16911309	1.7469	2.383774876	0.0731	2.08	0.490446	1030	11	1026	16	1017	42	101
b47	0.17370391	1.52285751	1.7588	2.744290589	0.0734	2.28	0.554918	1032	15	1030	18	1026	46	101
a14	0.17406807	1.73168284	1.8232	2.98037048	0.0760	2.43	0.581029	1034	17	1054	20	1094	49	95
b56	0.17454450	2.31441382	1.7439	8.616004991	0.0725	8.30	0.268618	1037	22	1025	57	999	169	104
c1	0.17471408	2.02075335	1.7319	2.955989216	0.0719	2.16	0.683613	1038	19	1020	19	983	44	106
a12	0.17524992	1.58656226	1.7646	2.790924585	0.0730	2.30	0.568472	1041	15	1033	18	1015	47	103
c32	0.17592995	0.96565408	1.8000	2.844775059	0.0742	2.68	0.339448	1045	9	1045	19	1047	54	100
c35	0.17624671	1.94398573	1.7834	2.62547116	0.0734	1.76	0.740433	1046	19	1039	17	1025	36	102
c44	0.17651575	1.36185119	1.7938	3.090780707	0.0737	2.77	0.440617	1048	13	1043	20	1033	56	101

c31	0.17681687	1.07974892	1.8120	2.520421037	0.0743	2.28	0.428400	1050	10	1050	17	1050	46	100
a21	0.17826503	2.37165603	1.8249	3.256753122	0.0742	2.23	0.728227	1057	23	1054	22	1048	45	101
b7	0.17832956	1.58505666	1.7662	2.238689103	0.0718	1.58	0.708029	1058	15	1033	15	981	32	108
c54	0.17844928	1.47339421	1.8632	3.351238986	0.0757	3.01	0.439657	1058	14	1068	22	1088	60	97
b10	0.18119913	2.49947523	1.8169	3.682761329	0.0727	2.70	0.678696	1074	25	1052	24	1006	55	107
b38	0.18205408	1.32439105	1.8920	3.369864776	0.0754	3.10	0.393010	1078	13	1078	23	1078	62	100
a11	0.18205827	2.09261962	1.9121	3.252160188	0.0762	2.49	0.643455	1078	21	1085	22	1100	50	98
b53	0.18250869	1.62329864	1.9218	5.077240712	0.0764	4.81	0.319721	1081	16	1089	34	1105	96	98
a29	0.18585533	1.49444498	1.8915	2.968343312	0.0738	2.56	0.503461	1099	15	1078	20	1036	52	106
a22	0.18663542	1.49044325	1.9572	2.425469355	0.0761	1.91	0.614497	1103	15	1101	16	1097	38	101
a7	0.19300495	1.61200645	2.0319	3.674370075	0.0764	3.30	0.438716	1138	17	1126	25	1104	66	103
c23	0.32653004	1.57873035	4.9941	3.508116843	0.1109	3.13	0.450022	1822	25	1818	30	1815	57	100
b36	0.32686101	1.35247835	5.1789	1.866081042	0.1149	1.29	0.724769	1823	22	1849	16	1879	23	97
c57	0.34483763	1.24947713	5.1727	2.011817539	0.1088	1.58	0.621069	1910	21	1848	17	1779	29	107
b11	0.35624328	1.70928189	6.0439	3.002573392	0.1230	2.47	0.569272	1964	29	1982	27	2001	44	98
b6	0.36819530	1.32906689	6.2480	2.369144061	0.1231	1.96	0.560990	2021	23	2011	21	2001	35	101
b19	0.38226344	1.64733397	6.4969	2.255885872	0.1233	1.54	0.730238	2087	29	2045	20	2004	27	104
b50	0.39208238	1.58638559	6.9635	2.348176999	0.1288	1.73	0.675582	2132	29	2107	21	2082	30	102
a2	0.40148729	1.37541084	7.0739	1.711603553	0.1278	1.02	0.803580	2176	25	2121	15	2068	18	105
c39	0.44880200	1.21190786	9.3259	2.065155272	0.1507	1.67	0.586836	2390	24	2371	19	2354	29	102
b28	0.47289902	2.18583790	11.6155	2.99718474	0.1781	2.05	0.729297	2496	45	2574	28	2636	34	95
b30	0.47642896	1.34045106	10.7244	1.984837126	0.1633	1.46	0.675346	2512	28	2500	19	2490	25	101
b26	0.48373663	2.06194521	11.1867	2.438164377	0.1677	1.30	0.845696	2544	43	2539	23	2535	22	100
c19	0.48490848	2.43795001	10.9240	2.751311113	0.1634	1.28	0.886105	2549	52	2517	26	2491	21	102
c22	0.49157553	2.28015954	10.8154	2.808977841	0.1596	1.64	0.811740	2577	49	2507	26	2451	28	105
b16	0.49286461	2.13627578	12.4027	2.562001401	0.1825	1.41	0.833831	2583	46	2635	24	2676	23	97
c50	0.52076762	1.11561244	12.9051	1.571058872	0.1797	1.11	0.710102	2702	25	2673	15	2650	18	102
a4	0.52891390	1.14534626	12.2042	1.609915065	0.1673	1.13	0.711433	2737	26	2620	15	2531	19	108

* Concordance (%), percentage concordance calculated from $^{207}Pb/^{206}Pb$ and $^{206}Pb/^{238}U$ ages (values greater than 100% are reverse discordant analyses).
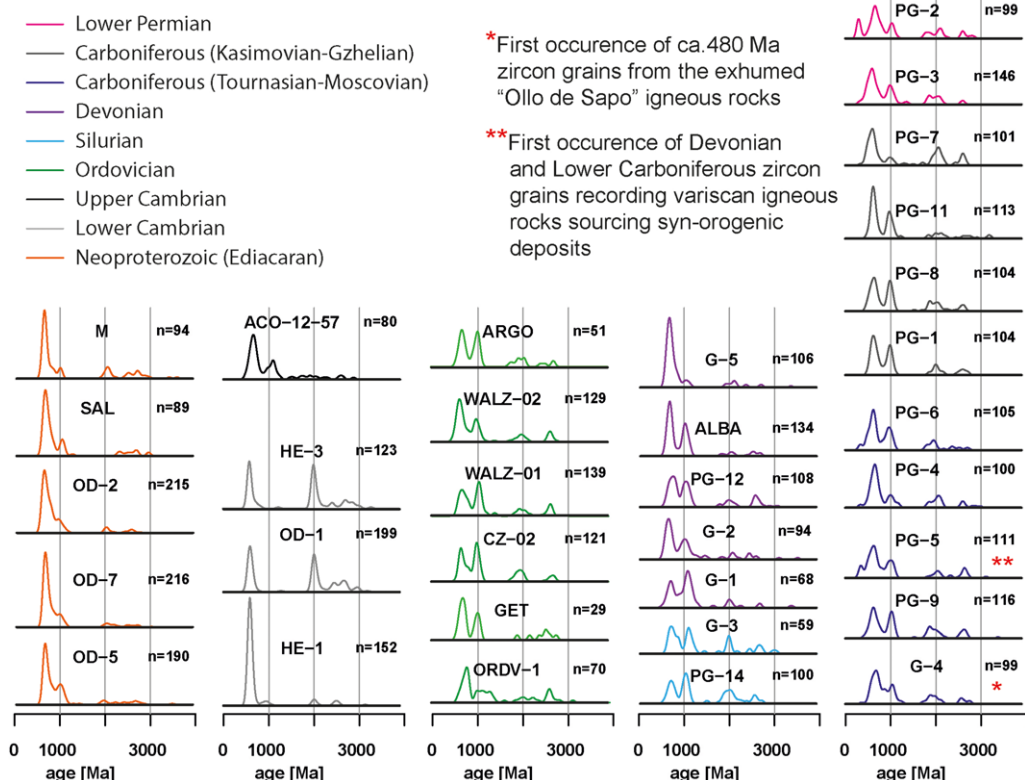
Fig. 7. Kernel density estimates of the 33 samples from the Cantabrian Zone used in this work, sorted by depositional age. Colours match sample labels in Figure 3 and the MDS plot in Figure 9.

superposition of the different curves (Fig. 8). This method is also a tool for visual comparison without the data smoothing made by PDPs or KDEs (Sircombe and Hazelton 2004; Vermeesch 2012). From Figure 8 it is noticeable that comparison with a large number of samples is difficult, and only the 'outliers' are easily recognizable, as is the case with some Cambrian samples from the studied dataset. This method, nevertheless, has the advantage that the cumulative curves can be easily compared, each with all of the others, and provide a numerical value for the similarity of all the performed comparisons. These comparisons made with statistical tests such as the Kolmogorov–Smirnov test, are intended to constrain whether a given pair of samples (i.e. zircon age populations, with or without uncertainties) have potentially been extracted from the same parent population (in geological terms, from the same source area).

Further to the above, the MDS approach provides a means for the comparison of samples based on the quantified pair-wise similarities of their detrital zircon ages based on Kolmogorov–Smirnov statistics,

and represents the vertical distance between two cumulative distribution functions or CADs (Cawood *et al.* 2012; Vermeesch 2017). MDS is used to transform a matrix of pairwise similarities, among all of the considered detrital zircon age populations, into cartesian coordinates in a two-dimensional space, where greater distances between samples represent a greater degree of dissimilarity between points on MDS diagrams (Vermeesch 2013; Wissink *et al.* 2018) and take on values between 0 (perfect match between two age distributions) and 1 (no overlap between two distributions). This method for comparison of detrital zircon ages in different samples is extremely useful for visualizing the degree of similarity among samples in a two-dimensional space (Vermeesch 2013; Spencer and Kirkland 2016).

In this work we have used IsoplotR (Vermeesch 2018) to produce the MDS configurations shown in Figure 9. This program can be run online (http://pieter-vermeesch.es.ucl.ac.uk/shiny/IsoplotR/); or offline under the R environment (https://www.r-project.org/). The MDS plots obtained using the data from the CZ and neighbouring areas provide insights into
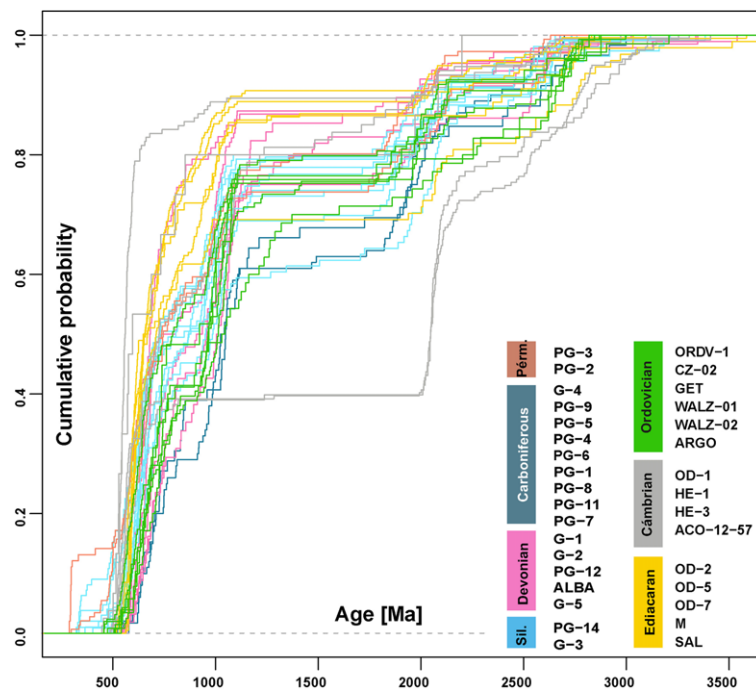
Fig. 8. Cumulative age distribution plots of the 33 samples from the Cantabrian Zone used in this work.

the similarities and differences between the samples (Fig. 9), especially when looked at along a time sequence from the Ediacaran to the Permian. The statistical relationships between the 33 samples obtained from the analysis of the MDS are shown in Figure 9, and together with the observation of the KDE curves (Fig. 7), CADs (Fig. 8) and the geological knowledge of the area, are interpreted and discussed in the following section.

Discussion

Figure 9a shows the MDS graphs constructed using the 33 samples used in this study. In the figure it can be seen that most of the samples cluster together and are around the point with coordinates (0, 0), indicating that the majority of them are very similar to each other. Only three samples show a clear difference from the rest, those corresponding to the early Cambrian samples (Herrería Fm., HE-1, OD-1 and HE-3; Fernández-Suárez et al. 2014; Zimmermann et al. 2015). This difference is basically justified as they are the only ones devoid of Tonian–Stenian zircon grains, and are also the only ones showing a large Paleoproterozoic peak (c. 2 Ga), indicating a change in the provenance area coincident with the end of the Cadomian cycle and the onset of the installation of a long-lived passive margin in the

north of Gondwana at the Ediacaran–Cambrian boundary (c. 540 Ma). In addition, the differences found within the statistically similar cluster formed by most of the samples can be used to decipher secular variations in the amount of zircons delivered to the margin from a given source at a given time or the importance of recycling during the Variscan orogeny.

In order to better understand the evolution of the sediment sources and the possible role of recycling, we have split the MSD graph (Fig. 9a) into four 'still frames' according to the evolution of the studied area (Fig. 9b.1–4) and will follow a description and discussion of the provenance evolution, focused on the detrital zircon ages through time.

We start with the oldest rocks (Fig. 9b.1), the Ediacaran thick pile of sediments and volcanic rocks related to a continental back-arc basin (Fernández-Suárez et al. 1998; Rubio-Ordóñez et al. 2015). They are well clustered together and statistically almost indistinguishable, with the only exception being sample M (Naidoo et al. 2018) characterized by the presence of a smaller amount of Tonian–Stenian zircon grains and a larger proportion of Paleoproterozoic zircon. The sources of these sediments have been interpreted to be derived from the Cadomian magmatic arc and the Saharan Metacraton (Abdelsalam et al. 2002) or the Arabian–Nubian Shield (Be'eri-Shlevin et al. 2012), which includes
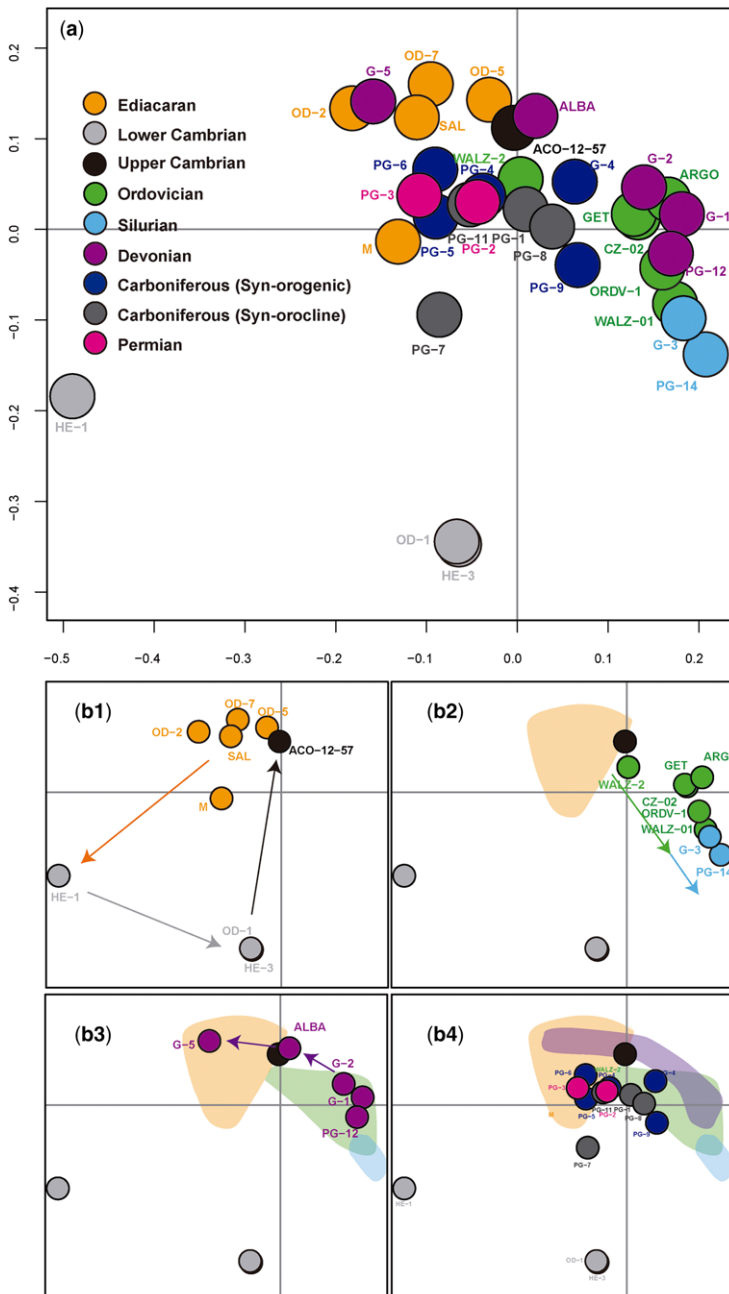
Fig. 9. (**a**) Multidimensional scaling plot of the 33 samples from the Cantabrian Zone used in this work.
(**b**) Sequential plots of the complete graph illustrating the temporal evolution of the provenance sources and the
recycling of the detrital zircon grains. See text for explanation.

Tonian–Stenian igneous rocks. Following the Edia-
caran, the unconformable lower Cambrian rocks
show a significant shift with respect to the Ediacaran
populations. Samples OD-1 and HE-3 (Fernández-

Suárez *et al.* 2014; Zimmermann *et al.* 2015) are stat-
istically identical, characterized by the presence of a
large proportion of Paleoproterozoic zircon grains
and the absence of Tonian–Stenian zircon grains.

On the contrary, sample HE-1 (Zimmermann *et al.* 2015) lacks the Paleoproterozoic population when compared with the other lower Cambrian samples. We argue that the reason for this difference is that sample HE-1 was collected very close to the base of the unit (just above the unconformity with the Ediacaran succession; Fig. 3), where sources were mainly local, recycling the detrital sediments and the volcanic rocks present in the underlying Ediacaran succession (Rubio Ordóñez *et al.* 2004). At this point, sediments with an origin in Paleoproterozoic zircon bearing rocks had not yet been significantly sourced to the newly formed passive margin from the Gondwana mainland. The large population of Paleoproterozoic zircon grains in the lower Cambrian rocks, classically assigned to sources in the West African Craton, suggests either a change in the palaeoposition of Iberia or an interruption of the Tonian–Stenian sources owing to modifications in the drainage system of northern Gondwana during the Ediacaran–Cambrian boundary. These variations were probably caused by a rift shoulder uplift, as will be discussed below, that precluded sediments arriving from the Gondwanan interior to the incipient passive margin. Erosion of the uplifted Gondwanan basement would have provided the large Paleoproterozoic zircon population.

In sample ACO-12-57 (Late Cambrian, Henderson *et al.* 2016), the zircon population is similar to those in the Ediacaran rocks, with a minor population of Paleoproterozoic zircon grains and a significant population of Tonian–Stenian zircon grains. This age pattern implies a recovery through time of the former sources of sediments that were active in the Ediacaran.

For the Ordovician and Silurian (Fig. 9b.2), the samples follow a trend in the MDS plot that corresponds to a differentiation from the Ediacaran and late Cambrian samples that is mostly driven by an increase in the proportion of zircon grains with Tonian–Stenian age. We interpret this increase to be related to the enlargement of the drainage basin of the river system sourcing sediments to the north Gondwana passive margin during this time, in a similar way to that proposed by Meinhold *et al.* (2013), or by environmentally triggered enhanced erosion (Avigad *et al.* 2005).

In the lower, middle and most of the upper Devonian (Fig. 9b.3), samples G-1, G-2 and PG-12 (Pastor-Galán *et al.* 2013*a*, *b*; Gutiérrez-Alonso *et al.* 2015), the detrital zircon population is identical to the population of the Ordovician and Silurian rocks, indicating a stable sedimentary supply, essentially from the same sources. The uppermost Devonian (samples ALBA and G-5) shows a trend of increasing similarity to the Ediacaran samples. We consider that the time-slice represented by samples ALBA and G5 characterizes the time when the first

effects of the Variscan orogeny can be detected in the CZ. The diminishing amount of Tonian–Stenian zircon grains reveals a sudden change in provenance from mostly/only continental Gondwana to sources located in the growing Variscan orogenic edifice. This orogenic pile was eroded to the west and south (in present-day coordinates) and the detritus was dumped from the advancing orogenic wedge into the fore-deep located in the CZ and/or from an alternative source coming from the erosion of the fore-bulge, located to the east, and shredding a mixture of older former passive-margin sequence detritus into the fore-deep (Agueda *et al.* 1991; Keller *et al.* 2008). The ongoing orogeny gave rise to sediments with a mixture of zircon grains that reflect the zircon spectra of all of the source rocks involved, especially of the Ediacaran ones.

The Carboniferous and Permian sediments (Fig. 9b.4) show a position of equidistant similarity to all of the samples from older rocks in the MDS plot. These sediments are all syn- to post-orogenic and have rather local sources, reflecting a mixture and recycling of all of the previous zircon grains present in the stratigraphic sequence described in this work. Three main changes in the zircon populations take place during this time, although they did not cause significant dissimilarity in the statistical parameters. The first occurrence in sample G-4 (Serpukhovian in age, asterisk in Fig. 7) of detrital zircon grains of early Ordovician age reveals the exhumation, erosion and transport of Ordovician igneous rocks present in the hinterland of the orogenic belt. This is an igneous suite known as 'Ollo de Sapo' (e.g. Díez-Montes *et al.* 2010) and the presence of zircon grains of this age suggests transport distances of at least 150 km. Another key point is the first occurrence in sample PG-5 (Bashkirian) of the first zircon grains with Devonian and early Carboniferous ages (double asterisk in Fig. 7). The latter zircon grains imply the exhumation of rocks from the Devonian ophiolites in the Variscan suture (e.g. Arenas *et al.* 2014) and the exhumation of early-orogenic igneous rocks. The Carboniferous igneous rocks correspond to the so-called 'Early granites', *c.* 340 Ma. (Gutiérrez-Alonso *et al.* 2018) and the anatectic granites generated during the orogenic collapse (*c.* 320 Ma, López-Moro *et al.* 2018). Exhumation of these rocks in the Variscan orogenic edifice of Iberia has been also identified through the use of detrital zircon grains in other syn-orogenic basins located in the hinterland (Martínez Catalán *et al.* 2016).

The Kasimovian–Gzelian samples (PG-1, PG-8, PG-11, PG-7; Pastor-Galán *et al.* 2013*a*, *b*) were collected in rocks representing local continental intramontane basins (Colmenero *et al.* 2008) and therefore reflect the mixture of the zircon populations of the local source rocks. Especially relevant is the case of PG-7, mostly sourced from Ediacaran

and lower Cambrian rocks and, therefore, showing an intermediate position between them in the MDS plot.

Finally, it is during the Permian (sample PG-2: Fig. 7) when zircon grains from the post-Variscan granites (310–290 Ma., Gutiérrez-Alonso *et al.* 2011) are incorporated into the sediments.

As described above, variations in detrital zircon populations through time in a given geological realm can be explained (and conversely reflect) in terms of the processes also recorded in other geological features like facies changes, large-scale sequences, etc. of the rocks in a stratigraphic succession. Whereas many previous works place their focus on interpretations invoking major palaeogeographic changes, including some of the authors' previous ones (see below), we propose that the detailed study of zircon age populations with appropriate statistical tools may help understand the tectonic evolution of a region without the necessity of involving large terrane displacements and ambiguous palaeogeographic reconstructions, but seeking interpretations that may require simpler and/or more local (lower-energy) processes, as shown in this study. The large amount of data compiled from samples used in this work, covering a continuous timespan, helps to minimize undersampling biases that could hinder identification of possible intermittent source changes through time (e.g. local sources and/or changes in the sedimentary routing), facilitating the presentation of consistent palaeogeographic models.

The major changes in the Ediacaran–Paleozoic succession studied via detrital zircon geochronology occur in the earliest Cambrian, when the first stages of rift-related extension are interpreted to have started. Within a rift basin scenario, one of the most relevant processes is the generation of rift shoulders, which are isostatically driven elevations at the rift flanks, where sedimentary routing gets diverted, or even inverted to the opposite direction, and detritus is transported away from the rift. In contrast, at this stage, the rift basin is filled only with sediments coming from exhumed basement rocks that crop out in the rift shoulders. The presence of a rift shoulder, therefore, precludes the transport of sediments from the former *c.* 1.0 Ga sources, located possibly somewhere in mainland Africa (e.g. Fernández-Suárez *et al.* 2014 and references therein), and causes a transient change to local sources. Rift shoulder-related sedimentary successions have been identified along both sides of the putative early stages of the rift that eventually became the Rheic ocean and are interpreted to be preserved in Morocco, on the Gondwanan side, and the Ardennes, on the Avalonian side (Álvaro *et al.* 2008; Herbosch *et al.* 2020 respectively). This interpretation leads to a more static view of the Ediacaran–Paleozoic geological history of the Gondwana-related realms in NW Iberia in which there is no need to invoke the role of large transcurrent faults that are not recognized in the geological record in this area (Fernández-Suárez *et al.* 2014).

Static scenarios have been proposed in other sectors of the Gondwana passive margin (i.e. the Bohemian Massif, Linnemann *et al.* 2004, Kroner and Romer 2013; Hajná *et al.* 2018; Stephan *et al.* 2019). These scenarios contrast with former ideas which imply large transcurrent terrane mobility to explain the variability in the detrital zircon content of the northern Gondwana margin (e.g. Fernández-Suárez *et al.* 2002*a*, *b*; Gutiérrez-Alonso *et al.* 2003; Díez Fernández *et al.* 2012*b*; Franke *et al.* 2019).

Moreover, the detrital zircon population homogeneity during the Late Cambrian, Ordovician, Silurian and most of the Devonian implies a continuous source of sediments, interpreted to reflect a location that never drifted from the Gondwana passive margin. This observation questions the location of Iberia in the so-called 'Armorican Terrane Assemblage' or Armorica microplate (e.g. Tait *et al.* 1997; Franke 2000; Stampfli *et al.* 2002), which is postulated to have drifted away from the Gondwana passive margin in Silurian times, in contrast with a more static evolution according to palaeogeobiographic constraints (Robardet 2003; Servais and Sintubin 2009) and the results obtained in this work.

Conclusions

Using MDS in 33 samples, we show the continuous source of sediments on the northern margin of Gondwana as it is preserved in an almost complete stratigraphic succession located in northern Iberia during *c.* 220 Ma (from *c.* 600 Ma, Ediacaran, to *c.* 380 Ma, Late Devonian) and the subsequent recycling of sediments during the Variscan orogeny. There is only a short period of time, in the early Cambrian, when the sediment sources change. This ephemeral change is coeval with the onset of the passive margin installation in the northern margin of Gondwana and, therefore, we interpret a change in sedimentary routing owing to a possible rift shoulder uplift and erosion of the local Gondwanan basement. We understand that the use of new statistical techniques when enough data are available through time in a given region, like the Cantabrian Zone, may lead to simpler (lower-energy) provenance evolution models that do not require large terrane displacements and ambiguous palaeogeographic reconstructions.

Data availability statement The authors confirm that the data supporting the findings of this study are available within the article.

References

Abdelsalam, M.G., Liégeois, J.P. and Stern, R.J. 2002. The saharan metacraton. *Journal of African Earth Sciences*, **34**, 119–136, https://doi.org/10.1016/S0899-5362 (02)00013-1

Agueda, J.A., Bahamonde, J.R. *et al*. 1991. Depositional environments in Westphalian coal-bearing successions of the Cantabrian Mountains, northwest Spain. *Bulletin de la Société Géologique de France*, **162**, 325–333.

Alonso, J.L., Marcos, A. and Suárez, A. 2009. Paleogeographic inversion resulting from large out of sequence breaching thrusts: the León Fault (Cantabrian Zone, NW Iberia). A new picture of the external Variscan Thrust Belt in the Ibero-Armorican Arc. *Geologica Acta*, **7**, 451–473, https://doi.org/10.1344/105. 000001449

Álvaro, J.J., Ezzouhairi, H., Ayad, N.A., Charif, A., Popov, L. and Ribeiro, M.L. 2008. Short-term episodes of carbonate productivity in a Cambrian uplifted rift shoulder of the Coastal Meseta, Morocco. *Gondwana*

Research, **14**, 410–428, https://doi.org/10.1016/j.gr. 2008.04.003

Andersen, T., Kristoffersen, M. and Elburg, M.A. 2018. Visualizing, interpreting and comparing detrital zircon age and Hf isotope data in basin analysis – a graphical approach. *Basin Research*, **30**, 132–147, https://doi. org/10.1111/bre.12245

Aramburu, C. and García-Ramos, J.C. 1993. La sedimentación cambro-ordovícica en la Zona Cantábrica (NO de España). *Trabajos de Geología, Universidad de Oviedo*, **19**, 45–75.

Arenas, R., Martínez, S.S., Gerdes, A., Albert, R., Díez Fernández, R. and Andonaegui, P. 2014. Re-interpreting the Devonian ophiolites involved in the Variscan suture: U–Pb and Lu–Hf zircon data of the Moeche Ophiolite (Cabo Ortegal Complex, NW Iberia). *International Journal of Earth Sciences*, **103**, 1385–1402, https://doi.org/10.1007/s00531-013-0880-x

Avigad, D., Sandler, A., Kolodner, K., Stern, R.J., McWilliams, M., Miller, N. and Beyth, M. 2005. Mass-production of Cambro–Ordovician quartz-rich sandstone as a consequence of chemical weathering of Pan-African terranes: environmental implications. *Earth and Planetary Science Letters*, **240**, 818–826, https://doi.org/10.1016/j.epsl.2005.09.021

Azor, A., Rubatto, D., Simancas, J.F., González Lodeiro, F., Martínez Poyatos, D., Martín Parra, L.M. and Matas, J. 2008. Rheic Ocean ophiolitic remnants in southern Iberia questioned by SHRIMP U–Pb zircon ages on the Beja–Acebuches amphibolites. *Tectonics*, **27**, TC5006, https://doi.org/10.1029/2008TC002306

Ballèvre, M., Martínez-Catalán, J.R., López-Carmona, A., Pitra, P., Abati, J., Díez Fernández, R. and Fernández-Suárez, J. 2014. Correlation of the nappe stack in the Ibero-Armorican arc across the Bay of Biscay: a joint French–Spanish project. *Geological Society, London, Special Publications*, **405**, 77–113, https://doi.org/ 10.1144/SP405.13

Be'eri-Shlevin, Y., Eyal, M., Eyal, Y., Whitehouse, M.J. and Litvinovsky, B. 2012. The Sa'al volcano-sedimentary complex (Sinai, Egypt): a latest Mesoproterozoic volcanic arc in the northern Arabian Nubian Shield. *Geology*, **40**, 403–406, https://doi.org/10. 1130/G32788.1

Bernárdez, E., Gutiérrez-Marco, J.C. and Hacar, M.P. 2006. Sedimentos glaciomarinos del Ordovícico terminal en la Zona Cantábrica (NO de España). *Geogaceta*, **40**, 239–242, http://sociedadgeologica.es/archivos/ geogacetas/Geo40/Geo40-60.pdf.

Bernárdez, E., Colmenar, J., Gutiérrez-Marco, J.C., Rábano, I. and Zamora, S. 2014. New peri-Gondwanan records of the Hirnantia Fauna in the latest Ordovician of Spain. *In*: Pankhurst, R.J., Castiñeiras y, P. and Sánchez, S. (eds) *Gondwana 15. North Meets South*. Abstracts Book, **15**. IGME, Madrid.

Cawood, P.A., Hawkesworth, C.J. and Dhuime, B. 2012. Detrital zircon record and tectonic setting. *Geology*, **40**, 875–878, https://doi.org/10.1130/G32945.1

Clariana, P., Valverde-Vaquero, P., Rubio-Ordóñez, A., Beranoaguirre, A. and García-Sansegundo, J. 2018. Pre-Variscan tectonic events and Late Ordovician magmatism in the Central Pyrenees: U–Pb age and Hf in zircon isotopic signature from subvolcanic sills in the Pallaresa massif. *Journal of Iberian geology*,

44, 589–601, https://doi.org/10.1007/s41513-018-0076-0

Colmenero, J.R., Fernández, L.P., Moreno, C., Bahamonde, J.R., Barba, P., Heredia, N. and González, F. 2002. Carboniferous. *In*: Gibbons, W. and Moreno, T. (eds) *The Geology of Spain*. Geological Society, London, 93–116.

Colmenero, J.R., Suárez-Ruiz, I., Fernández-Suárez, J., Barba, P. and Llorens, T. 2008. Genesis and rank distribution of Upper Carboniferous coal basins in the Cantabrian Mountains, Northern Spain. *International Journal of Coal Geology*, **76**, 187–204, https://doi.org/10.1016/j.coal.2008.08.004

Condie, K.C. and Aster, R.C. 2010. Episodic zircon age spectra of orogenic granitoids: the supercontinent connection and continental growth. *Precambrian Research*, **180**, 227–236, https://doi.org/10.1016/j.precamres.2010.03.008

Dallmeyer, R.D., Martínez Catalan, J.R. *et al.* 1997. Diachronous Variscan tectonothermal activity in the NW Iberian Massif: evidence from Ar-40/Ar-39 dating of regional fabrics. *Tectonophysics*, **277**, 307–337, https://doi.org/10.1016/S0040-1951(97)00035-8

Dias da Silva, Í., González Clavijo, E. and Díez-Montes, A. 2020. The collapse of the Variscan belt: a Variscan lateral extrusion thin-skinned structure in NW Iberia. *International Geology Review*, 1–37, https://doi.org/10.1080/00206814.2020.1719544

Díez Fernández, R., Castiñeiras, P. and Gómez Barreiro, J. 2012*a*. Age constraints on Lower Paleozoic convection system: magmatic events in the NW Iberian Gondwana margin. *Gondwana Research*, **21**, 1066–1079, https://doi.org/10.1016/j.gr.2011.07.028

Díez Fernández, R., Martinez Catalan, J.R., Arenas, R., Abati, J., Gerdes, A. and Fernández-Suárez, J. 2012*b*. U–Pb detrital zircon analysis of the lower allochthon of NW Iberia: age constraints, provenance and links with the Variscan mobile belt and Gondwanan cratons. *Journal of the Geological Society*, **169**, 655–665, https://doi.org/10.1144/jgs2011-146

Díez Fernández, R., Arenas, R. *et al.* 2016. Tectonic evolution of Variscan Iberia: gondwana–Laurussia collision revisited. *Earth-Science Reviews*, **162**, 269–292, https://doi.org/10.1016/j.earscirev.2016.08.002

Díez-Montes, A., Martínez-Catalán, J.R. and Bellido Mulas, F. 2010. Role of the Ollo de Sapo massive felsic volcanism of NW Iberia in the Early Ordovician dynamics of northern Gondwana. *Gondwana Research*, **17**, 363–376, https://doi.org/10.1016/j.gr.2009.09.001

Domeier, M. and Torsvik, T.H. 2014. Plate tectonics in the late Paleozoic. *Geoscience Frontiers*, **5**, 303–350, https://doi.org/10.1016/j.gsf.2014.01.002

Edel, J.B., Schulmann, K., Lexa, O. and Lardeaux, J.M. 2018. Late Palaeozoic palaeomagnetic and tectonic constraints for amalgamation of Pangea supercontinent in the European Variscan belt. *Earth-science reviews*, **177**, 589–612, https://doi.org/10.1016/j.earscirev.2017.12.007

Fernández-Lozano, J., Pastor-Galán, D., Gutiérrez-Alonso, G. and Franco, P. 2016. New kinematic constraints on the Cantabrian orocline: a paleomagnetic study from the Peñalba and Truchas synclines, NW Spain. *Tectonophysics*, **681**, 195–208, https://doi.org/10.1016/j.tecto.2016.02.019

Fernández-Suárez, J., Gutiérrez-Alonso, G., Jenner, G.A. and Jackson, S.E. 1998. Geochronology and geochemistry of the Pola de Allande granitoids (northern Spain): their bearing on the Cadomian-Avalonian evolution of northwest Iberia. *Canadian Journal of Earth Sciences*, **35**, 1439–1453, https://doi.org/10.1139/e98-074

Fernández-Suárez, J., Gutiérrez-Alonso, G., Jenner, G.A. and Tubrett, M.N. 1999. Crustal sources in Lower Palaeozoic rocks from NW Iberia: insights from laser ablation U–Pb ages of detrital zircons. *Journal of the Geological Society*, **156**, 1065–1068, https://doi.org/10.1144/gsjgs.156.6.1065

Fernández-Suárez, J., Gutiérrez-Alonso, G., Jenner, G.A. and Tubrett, M.N. 2000. New ideas on the Proterozoic–Early Palaeozoic evolution of NW Iberia: insights from U–Pb detrital zircon ages. *Precambrian Research*, **102**, 185–206, https://doi.org/10.1016/S0301-9268(00)00065-6

Fernández-Suárez, J., Gutiérrez-Alonso, G. and Jeffries, T.E. 2002*a*. The importance of along-margin terrane transport in northern Gondwana: insights from detrital zircon parentage in Neoproterozoic rocks from Iberia and Brittany. *Earth and Planetary Science Letters*, **204**, 75–88, https://doi.org/10.1016/S0012-821X(02)00963-9

Fernández-Suárez, J., Gutiérrez-Alonso, G., Cox, R. and Jenner, G.A. 2002*b*. Assembly of the Armorica microplate: a strike-slip terrane delivery? Evidence from U–Pb ages of detrital zircons. *The Journal of geology*, **110**, 619–626, https://doi.org/10.1086/341760

Fernández-Suárez, J., Gutiérrez-Alonso, G., Pastor-Galán, D., Hofmann, M., Murphy, J.B. and Linnemann, U. 2014. The Ediacaran–Early Cambrian detrital zircon record of NW Iberia: possible sources and paleographic constraints. *International Journal of Earth Sciences*, **103**, 1335–1357, https://doi.org/10.1007/s00531-013-0923-3

Franke, W. 2000. The mid-European segment of the Variscides: tectonostratigraphic units, terrane boundaries and plate tectonic evolution. *Geological Society, London, Special Publications*, **179**, 35–61, https://doi.org/10.1144/GSL.SP.2000.179.01.05

Franke, W., Cocks, L.R.M. and Torsvik, T.H. 2017. The Palaeozoic Variscan oceans revisited. *Gondwana Research*, **48**, 257–284, https://doi.org/10.1016/j.gr.2017.03.005

Franke, W., Cocks, L.R.M. and Torsvik, T.H. 2019. Detrital zircons and the interpretation of palaeogeography, with the Variscan Orogeny as an example. *Geological Magazine*, **157**, 690–694, https://doi.org/10.1017/S0016756819000943

Frei, D. and Gerdes, A. 2009. Precise and accurate *in situ* U–Pb dating of zircon with high sample throughput by automated LA–SF–ICP–MS. *Chemical Geology*, **261**, 261–270, https://doi.org/10.1016/j.chemgeo.2008.07.025

Gallastegui, G., Aramburu, C., Barba, P., Fernández, L.P. and Cuesta, A. 1992. El vulcanismo del Paleozoico Inferior de la Zona Cantábrica (NO de España). *In*: Rabano, I., Gutiérrez-Marco, J.C. and Saavedra, J. (eds) *El Paleozoico Inferior de Ibero-América*. Universidad de Extremadura, 435–452.

García-Ramos, J.C. and Colmenero, J.R. 1981. Evolución sedimentaria y paleogeográfica durante el Devónico

en la Cordillera Cantábrica. *Revista de la Real Academia de Ciencias Exactas, Físicas y Naturales*, **2**, 61–76.

García-Ramos, J.C., Aramburu, C. and Brime, C. 1984. Kaolin tonstein of volcanincs ash origin in the Lower Ordovician of the Cantabrian Mountains (NW Spain). *Trabajos de Geología, Universidad de Oviedo*, **14**, 27–35.

Gutiérrez-Alonso, G. 1996. Strain partitioning in the footwall of the Somiedo Nappe: structural evolution of the Narcea Tectonic Window, NW Spain. *Journal of Structural Geology*, **18**, 1217–1229, https://doi.org/10.1016/S0191-8141(96)00034-X

Gutiérrez-Alonso, G., Fernández-Suárez, J., Jeffries, T.E., Jenner, G.A., Tubrett, M.N., Cox, R. and Jackson, S.E. 2003. Terrane accretion and dispersal in the northern Gondwana margin. An Early Paleozoic analogue of a long-lived active margin. *Tectonophysics*, **365**, 221–232, https://doi.org/10.1016/S0040-1951(03)00023-4

Gutiérrez-Alonso, G., Fernández-Suárez, J. and Weil, A.B. 2004. Orocline triggered lithospheric delamination. *Geological Society of America, Special Papers*, **383**, 121–130, https://doi.org/10.1130/0-8137-2383-3(2004)383[121:OTLD]2.0.CO;2

Gutiérrez-Alonso, G., Fernández-Suárez, J., Gutiérrez-Marco, J.C., Corfu, F., Murphy, J.B., Suárez, M. and Linnemann, U. 2007. U–Pb depositional age for the upper Barrios Formation (Armorican Quartzite facies) in the Cantabrian zone of Iberia: implications for stratigraphic correlation and paleogeography. *Geological Society of America, Special Papers*, **423**, 287–296, https://doi.org/10.1130/2007.2423(13)

Gutiérrez-Alonso, G., Murphy, J.B., Fernández-Suárez, J. and Hamilton, M.A. 2008. Rifting along the northern Gondwana margin and the evolution of the Rheic Ocean: a Devonian age for the El Castillo volcanic rocks (Salamanca, Central Iberian Zone). *Tectonophysics*, **461**, 157–165, https://doi.org/10.1016/j.tecto.2008.01.013

Gutiérrez-Alonso, G., Fernández-Suárez, J. *et al.* 2011. Diachronous post-orogenic magmatism within a developing orocline in Iberia, European Variscides. *Tectonics*, **30**, TC002845, https://doi.org/10.1029/2010TC002845

Gutiérrez-Alonso, G., Fernández-Suárez, J. *et al.* 2015. Significance of detrital zircons in Siluro-Devonian rocks from Iberia. *Journal of the Geological Society*, **172**, 309–322, https://doi.org/10.1144/jgs2014-118

Gutiérrez-Alonso, G., Gutiérrez-Marco, J.C., Fernández-Suárez, J., Bernárdez, E. and Corfu, F. 2016. Was there a super-eruption on the Gondwanan coast 477 Ma ago? *Tectonophysics*, **681**, 85–94, https://doi.org/10.1016/j.tecto.2015.12.012

Gutiérrez-Alonso, G., Fernández-Suárez, J., López-Carmona, A. and Gärtner, A. 2018. Exhuming a cold case: the early granodiorites of the northwest Iberian Variscan belt – a Visean magmatic flare-up? *Lithosphere*, **10**, 194–216, https://doi.org/10.1130/L706.1

Gutiérrez-Marco, J.C., Ghienne, J.F., Bernárdez, E. and Hacar, M.P. 2010. Did the Late Ordovician African ice sheet reach Europe? *Geology*, **38**, 279–282, https://doi.org/10.1130/G30430.1

Gutiérrez-Marco, J.C., Piçarra, J.M. *et al.* 2019. Early Ordovician–Devonian passive margin stage in the Gondwanan units of the Iberian Massif. *In*: The Geology of Iberia: A Geodynamic Approach. Springer, Chamonix, Regional Geology Reviews, **2**, 75–98.

Hajná, J., Žák, J., Dörr, W., Kachlík, V. and Sláma, J. 2018. New constraints from detrital zircon ages on prolonged, multiphase transition from the Cadomian accretionary orogen to a passive margin of Gondwana. *Precambrian Research*, **317**, 159–178, https://doi.org/10.1016/j.precamres.2018.08.013

Hatcher, R.D. 2010. The Appalachian orogen: a brief summary. *Geological Society of America Memoirs*, **206**, 1–19, https://doi.org/10.1130/2010.1206(01)

Heinz, W., Loeschke, J. and Vavra, G. 1985. Phreatomagmatic volcanism during the Ordovician of the Cantabrian Mountains (NW Spain). *Geologische Rundschau*, **74**, 623–639, https://doi.org/10.1007/BF01821217

Henderson, B.J., Collins, W.J., Murphy, J.B., Gutierrez-Alonso, G. and Hand, M. 2016. Gondwanan basement terranes of the Variscan–Appalachian orogen: Baltican, Saharan and West African hafnium isotopic fingerprints in Avalonia, Iberia and the Armorican Terranes. *Tectonophysics*, **681**, 278–304, https://doi.org/10.1016/j.tecto.2015.11.020

Herbosch, A., Liégeois, J.P., Gärtner, A., Hofmann, M. and Linnemann, U. 2020. The Stavelot-Venn Massif (Ardenne, Belgium), a rift shoulder basin ripped off the West African craton: cartography, stratigraphy, sedimentology, new U–Pb on zircon ages, geochemistry and Nd isotopes evidence. *Earth-Science Reviews*, **203**, 103142, https://doi.org/10.1016/j.earscirev.2020.103142

Hibbard, J.P., van Staal, C.R. and Rankin, D.W. 2010. Comparative analysis of the geological evolution of the northern and southern Appalachian orogen: late Ordovician-Permian. *Geological Society of America Memoirs*, **206**, 51–69, https://doi.org/10.1130/2010.1206(03)

Jackson, S.E., Pearson, N.J., Griffin, W.L. and Belousova, E.A. 2004. The application of laser ablation-inductively coupled plasma-mass spectrometry to in situ U–Pb zircon geochronology. *Chemical Geology*, **211**, 47–69, https://doi.org/10.1016/j.chemgeo.2004.06.017

Julivert, M. 1971. Décollement tectonics in the Hercynian Cordillera of northwest Spain. *American Journal of Science*, **270**, 1–29, https://doi.org/10.2475/ajs.270.1.1

Julivert, M. 1978. Hercynian orogeny and carboniferous paleogeography in NW Spain: a model of deformation-sedimentation relationships. *Zeitschrift der Deutschen Geologischen Gesellschaft*, **129**, 565–592.

Keller, M., Bahlburg, H., Reuther, C.D. and Weh, A. 2007. Flexural to broken foreland basin evolution as a result of Variscan collisional events in northwestern Spain. *Geological Society of America Memoirs*, **200**, 489–510, https://doi.org/10.1130/2007.1200(25)

Keller, M., Bahlburg, H. and Reuther, C.D. 2008. The transition from passive to active margin sedimentation in the Cantabrian Mountains, Northern Spain: Devonian or Carboniferous? *Tectonophysics*, **461**, 414–427, https://doi.org/10.1016/j.tecto.2008.06.022

Kroner, U. and Romer, R.L. 2013. Two plates – Many subduction zones: the Variscan orogeny reconsidered. *Gondwana Research*, **24**, 298–329, https://doi.org/10.1016/j.gr.2013.03.001

Linnemann, U., McNaughton, N.J., Romer, R.L., Gehmlich, M., Drost, K. and Tonk, C. 2004. West African provenance for Saxo-Thuringia (Bohemian Massif): did Armorica ever leave pre-Pangean Gondwana? U/Pb-SHRIMP zircon evidence and the Nd-isotopic record. *International Journal of Earth Sciences*, **93**, 683–705, https://doi.org/10.1007/s00531-004-0413-8

Linnemann, U., Pereira, F., Jeffries, T.E., Drost, K. and Gerdes, A. 2008. The Cadomian Orogeny and the opening of the Rheic Ocean: the diacrony of geotectonic processes constrained by LA–ICP–MS U–Pb zircon dating (Ossa-Morena and Saxo-Thuringian Zones, Iberian and Bohemian Massifs). *Tectonophysics*, **461**, 21–43, https://doi.org/10.1016/j.tecto.2008.05.002

López-Carmona, A., Abati, J., Pitra, P. and Lee, J.K. 2014. Retrogressed lawsonite blueschists from the NW Iberian Massif: $P–T–t$ constraints from thermodynamic modelling and $^{40}Ar/^{39}Ar$ geochronology. *Contributions to Mineralogy and Petrology*, **167**, 987.19-439, https://doi.org/10.1007/s00410-014-0987-5

López-Moro, F.J., López-Plaza, M., Gutiérrez-Alonso, G., Fernández-Suárez, J., López-Carmona, A., Hofmann, M. and Romer, R.L. 2018. Crustal melting and recycling: geochronology and sources of Variscan syn-kinematic anatectic granitoids of the Tormes Dome (Central Iberian Zone). A U–Pb LA–ICP–MS study. *International Journal of Earth Sciences*, **107**, 985–1004, https://doi.org/10.1007/s00531-017-1483-8

Ludwig, K.R. 1998. On the treatment of concordant uranium–lead ages. *Geochimica et Cosmochimica Acta*, **62**, 665–676, https://doi.org/10.1016/S0016-7037(98)00059-3

Ludwig, K.R. 2001. Isoplot/Ex version 2.49: *a geochronology toolkit for Microsoft Excel. Berkeley Geochronology Center, Special Publications*, **55**, http://www.bgc.org/isoplot_etc/isoplot.html

Marcos, A. and Pulgar, J.A. 1982. An approach to the tectonostratigraphic evolution of the Cantabrian foreland thrust and fold belt, Hercynian Cordillera of NW Spain. *Neues Jahrbuch für Geologie und Paläontologie. Abhandlungen*, **163**, 256–260.

Martínez Catalán, J.R., Fernández-Suárez, J., Jenner, G.A., Belousova, E. and Díez Montes, A. 2004. Provenance constraints from detrital zircon U–Pb ages in the NW Iberian Massif: implications for Palaeozoic plate configuration and Variscan evolution. *Journal of the Geological Society*, **161**, 463–476, https://doi.org/10.1144/0016-764903-054

Martínez Catalán, J.R., Arenas, R. *et al.* 2007. Space and time in the tectonic evolution of the northwestern Iberian Massif: implications for the Variscan belt. *Geological Society of America Memoirs*, **200**, 403–423, https://doi.org/10.1130/2007.1200(21)

Martínez Catalán, J.R., González Clavijo, E., Meireles, C., Díez Fernández, R. and Bevis, J. 2016. Relationships between syn-orogenic sedimentation and nappe emplacement in the hinterland of the Variscan belt in NW Iberia deduced from detrital zircons. *Geological Magazine*, **153**, 38–60, https://doi.org/10.1017/S001675681500028X

Martínez Catalán, J.R., Collett, S., Schulmann, K., Aleksandrowski, P. and Mazur, S. 2019. Correlation of allochthonous terranes and major tectonostratigraphic domains between NW Iberia and the Bohemian Massif, European Variscan belt. *International Journal of Earth Sciences*, **109**, 1105–1131, https://doi.org/10.1007/s00531-019-01800-z

Martínez-García, E. 1991. Hercynian synorogenic and postorogenic sucessions in the Cantabrian and Palentian Zobes, NW Spain. Comparisons with other western European ocurrences. *Giornale di Geologia*, **53**, 209–228.

Matte, P. 1986. Tectonics and plate tectonics model for the Variscan belt of Europe. *Tectonophysics*, **126**, 329–374, https://doi.org/10.1016/0040-1951(86)90237-4

Mazur, S., Aleksandrowski, P. *et al.* 2010. Uplift and late orogenic deformation of the Central European Variscan belt as revealed by sediment provenance and structural record in the Carboniferous foreland basin of western Poland. *International Journal of Earth Sciences*, **99**, 47–64, https://doi.org/10.1007/s00531-008-0367-3

Meinhold, G., Morton, A.C. and Avigad, D. 2013. New insights into peri-Gondwana paleogeography and the Gondwana super-fan system from detrital zircon U–Pb ages. *Gondwana Research*, **23**, 661–665, https://doi.org/10.1016/j.gr.2012.05.003

Merino-Tomé, O., Gutiérrez-Alonso, G., Villa, E., Fernández-Suárez, J., Llaneza, J.M. and Hofmann, M. 2017. LA–ICP–MS U–Pb dating of Carboniferous ash layers in the Cantabrian Zone (N Spain): stratigraphic implications. *Journal of the Geological Society*, **174**, 836–849, https://doi.org/10.1144/jgs2016-119

Murphy, J.B., Pisarevsky, S.A., Nance, R.D. and Keppie, J.D. 2004*a*. Neoproterozoic–Early Paleozoic evolution of peri-Gondwanan terranes: implications for Laurentia-Gondwana connections. *International Journal of Earth Sciences*, **93**, 659–682, https://doi.org/10.1007/s00531-004-0412-9

Murphy, J.B., Fernández-Suárez, J., Jeffries, T. and Strachan, R. 2004*b*. U–Pb (LA–ICP–MS) dating of detrital zircons from Cambrian clastic rocks in Avalonia: erosion of a Neoproterozoic arc along the northern Gondwanan margin. *Journal of the Geological Society*, **161**, 243–254, https://doi.org/10.1144/0016-764903-064

Murphy, J.B., Gutierrez-Alonso, G. *et al.* 2006. Origin of the Rheic Ocean: rifting along a Neoproterozoic suture? *Geology*, **34**, 325–328, https://doi.org/10.1016/j.tecto.2008.03.013

Murphy, J.B., Gutiérrez-Alonso, G., Fernández-Suárez, J. and Braid, J.A. 2008. Probing crustal and mantle lithosphere origin through Ordovician volcanic rocks along the Iberian passive margin of Gondwana. *Tectonophysics*, **461**, 166–180, https://doi.org/10.1016/j.tecto.2008.03.013

Naidoo, T., Zimmermann, U., Vervoort, J. and Tait, J. 2018. Evidence of early Archean crust in northwest Gondwana, from U–Pb and Hf isotope analysis of detrital zircon, in Ediacaran surpacrustal rocks of northern Spain. *International Journal of Earth Sciences*, **107**, 409–429, https://doi.org/10.1007/s00531-017-1500-y

Nance, R.D. and Murphy, J.B. 2019. Supercontinents and the case for Pannotia. *Geological Society, London, Special Publications*, **470**, 65–86, https://doi.org/10.1144/SP470.5

Nance, R.D., Gutiérrez-Alonso, G. *et al.* 2010. Evolution of the Rheic ocean. *Gondwana Research*, **17**, 194–222, https://doi.org/10.1016/j.gr.2009.08.001

Navidad, M., Castiñeiras, P., Casas, J.M., Liesa, M., Belousova, E., Proenza, J. and Aiglsperger, T. 2018. Ordovician magmatism in the Eastern Pyrenees: implications for the geodynamic evolution of northern Gondwana. *Lithos*, **314**, 479–496, https://doi.org/10.1016/j.lithos.2018.06.019

Palacios, T. 2015. Acritarch assemblages from the Oville and Barrios Formations, northern Spain: a pilot proposal of a middle Cambrian (Series 3) acritarch biozonation in northwestern Gondwana. *Review of Palaeobotany and Palynology*, **219**, 71–105, https://doi.org/10.1016/j.revpalbo.2015.03.008

Pastor-Galán, D., Gutiérrez-Alonso, G. and Weil, A.B. 2011. Orocline timing through joint analysis: insights from the Ibero-Armorican Arc. *Tectonophysics*, **507**, 31–46, https://doi.org/10.1016/j.tecto.2011.05.005

Pastor-Galán, D., Gutiérrez-Alonso, G., Murphy, J.B., Fernández-Suárez, J., Hofmann, M. and Linnemann, U. 2013*a*. Provenance analysis of the Paleozoic sequences of the northern Gondwana margin in NW Iberia: passive margin to Variscan collision and orocline development. *Gondwana Research*, **23**, 1089–1103, https://doi.org/10.1016/j.gr.2012.06.015

Pastor-Galán, D., Gutiérrez-Alonso, G., Fernández-Suárez, J., Murphy, J.B. and Nieto, F. 2013*b*. Tectonic evolution of NW Iberia during the Paleozoic inferred from the geochemical record of detrital rocks in the Cantabrian Zone. *Lithos*, **182**, 211–228, https://doi.org/10.1016/j.lithos.2013.09.007

Pastor-Galán, D., Nance, R.D., Murphy, J.B. and Spencer, C.J. 2019. Supercontinents: myths, mysteries, and milestones. *Geological Society, London, Special Publications*, **470**, 39–64, https://doi.org/10.1144/SP470.16

Pastor-Galán, D., Gutiérrez-Alonso, G. and Weil, A.B. 2020, The enigmatic curvature of Central Iberia and its puzzling kinematics. *Solid Earth*, **11**, 1247–1273, https://doi.org/10.5194/se-11-1247-2020

Pereira, M.F., Solá, A.R., Chichorro, M., Lopes, L., Gerdes, A. and Silva, J.B. 2012. North-Gondwana assembly, break-up and paleogeography: U–Pb isotope evidence from detrital and igneous zircons of Ediacaran and Cambrian rocks of SW Iberia. *Gondwana Research*, **22**, 866–881, https://doi.org/10.1016/j.gr.2012.02.010

Pérez-Cáceres, I., Poyatos, D.M., Simancas, J.F. and Azor, A. 2017. Testing the Avalonian affinity of the South Portuguese Zone and the Neoproterozoic evolution of SW Iberia through detrital zircon populations. *Gondwana Research*, **42**, 177–192, https://doi.org/10.1016/j.gr.2016.10.010

Pérez-Estaún, A., Bastida, F. *et al.* 1988. A thin-skinned tectonics model for an arcuate fold and thrust belt: the Cantabrian Zone (Variscan Ibero-Armorican Arc). *Tectonics*, **7**, 517–537, https://doi.org/10.1029/TC007i003p00517

Robardet, M. 2003. The Armorica 'microplate': fact or fiction? Critical review of the concept and contradictory palaeobiogeographical data. *Palaeogeography, Palaeoclimatology, Palaeoecology*, **195**, 125–148, https://doi.org/10.1016/S0031-0182(03)00305-5

Rodríguez, J., Cosca, M.A., Gil Ibarguchi, J.I. and Dallmeyer, R.D. 2003. Strain partitioning and preservation of $^{40}Ar/^{39}Ar$ ages during Variscan exhumation of a subducted crust (Malpica–Tui complex, NW Spain). *Lithos*, **70**, 111–139, https://doi.org/10.1016/S0024-4937(03)00095-1

Rodríguez-Fernández, L.R., García-Alcalde, J.L. and Menéndez-Álvarez, J.R. 1985. La sucesión del Devónico Superior y Carbonífero Inferior en el Sinclinal de Alba (León, NO de España). X Congreso Internacional de Estratigrafía y Geología del Carbonífero, Madrid, Spain. Instituto Geológico y Minero de España, Madrid, **1**, 133–144.

Rubio Ordóñez, Á., Barba, P., Cuesta, A., Gallastegui, G., Suárez, O., Ugidos, J.M. and Valladares, M.I. 2004. Los cantos volcánicos del conglomerado basal de la Fm. Herrería: evidencias de un volcanismo Neoproterozoico en la base del Cámbrico. *Geogaceta*, **36**, 11–14, http://www.sociedadgeologica.es/archivos/geogacetas/Geo36/Art03.pdf.

Rubio-Ordóñez, Á., Gutiérrez-Alonso, G., Valverde-Vaquero, P., Cuesta, A., Gallastegui, G., Gerdes, A. and Cárdenes, V. 2015. Arc-related Ediacaran magmatism along the northern margin of Gondwana: geochronology and isotopic geochemistry from northern Iberia. *Gondwana Research*, **27**, 216–227, https://doi.org/10.1016/j.gr.2013.09.016

Rubio Pascual, F.J., Arenas, R., Martínez Catalán, J.R., Rodríguez Fernández, L.R. and Wijbrans, J.R. 2013. Thickening and exhumation of the Variscan roots in the Iberian Central System: tectonothermal processes and $^{40}Ar/^{39}Ar$ ages. *Tectonophysics*, **587**, 207–221, https://doi.org/10.1016/j.tecto.2012.10.005

Sánchez-García, T., Quesada, C., Bellido, F., Dunning, G.R. and García del Tanago, J. 2008. Two step magma flooding of the upper crust during rifting: the Early Paleozoic of the Ossa Morena Zone (SW Iberia). *Tectonophysics*, **461**, 72–90, https://doi.org/10.1016/j.tecto.2008.03.006

Sánchez-García, T., Chichorro, M. *et al.* 2019. The Cambrian–Early Ordovician rift stage in the Gondwanan units of the Iberian Massif. *In*: Quesada, C. and Oliveira, J.T. (eds) *The Geology of Iberia: A Geodynamic Approach.* Springer, Chamonix, Regional Geology Reviews, **2**, 27–74, https://doi.org/10.1007/978-3-030-10519-8_2

Santos Zalduegui, J.F., Schärer, U., Gil Ibarguchi, J. and Girardeau, J. 1996. Origin and evolution of the Paleozoic Cabo Ortegal ultramafic-mafic complex (NW Spain): U–Pb, Rb–Sr and Pb–Pb isotope data. *Chemical Geology*, **129**, 281–304, https://doi.org/10.1016/0009-2541(95)00144-1

Saylor, J.E. and Sundell, K.E. 2016. Quantifying comparison of large detrital geochronology data sets. *Geosphere*, **12**, 203–220, https://doi.org/10.1130/GES01237.1

Servais, T. and Sintubin, M. 2009. Avalonia, Armorica, Perunica: terranes, microcontinents, microplates or palaeobiogeographical provinces? *Geological Society, London, Special Publications*, **325**, 103–115, https://doi.org/10.1144/SP325.5

Shaw, J., Johnston, S.T., Gutiérrez-Alonso, G. and Weil, A.B. 2012. Oroclines of the Variscan orogen of Iberia: paleocurrent analysis and paleogeographic implications. *Earth and Planetary Science Letters*, **329**, 60–70, https://doi.org/10.1016/j.epsl.2012.02.014

Shaw, J., Gutiérrez-Alonso, G., Johnston, S.T. and Pastor-Galán, D. 2014. Provenance variability along the Early Ordovician north Gondwana margin: paleogeographic and tectonic implications of U–Pb detrital zircon ages from the Armorican Quartzite of the Iberian Variscan belt. *Geological Society of America Bulletin*, **126**, 702–719, https://doi.org/10.1130/B30935.1

Shaw, J., Johnston, S.T. and Gutiérrez-Alonso, G. 2015. Orocline formation at the core of Pangea: a structural study of the Cantabrian orocline, NW Iberian Massif. *Lithosphere*, **7**, 653–661, https://doi.org/10.1130/L461.1

Sircombe, K.N. and Hazelton, M.L. 2004. Comparison of detrital zircon age distributions by kernel functional estimation. *Sedimentary Geology*, **171**, 91–111, https://doi.org/10.1016/j.sedgeo.2004.05.012

Spencer, C.J. and Kirkland, C.L. 2016. Visualizing the sedimentary response through the orogenic cycle: a multidimensional scaling approach. *Lithosphere*, **8**, 29–37, https://doi.org/10.1130/L479.1

Stacey, J.T. and Kramers, I. 1975. Approximation of terrestrial lead isotope evolution by a two-stage model. *Earth and Planetary Science Letters*, **26**, 207–221, https://doi.org/10.1016/0012-821X(75)90088-6

Stampfli, G.M., von Raumer, J.F. and Borel, G.D. 2002. Paleozoic evolution of pre-Variscan terranes: from Gondwana to the Variscan collision. *Geological Society of America, Special Papers*, **364**, 263–280, https://doi.org/10.1130/0-8137-2364-7.263

Stephan, T., Kroner, U., Romer, R.L. and Rösel, D. 2019. From a bipartite Gondwana shelf to an arcuate Variscan belt: the early Paleozoic evolution of northern Peri-Gondwana. *Earth-science Reviews*, **192**, 491–512, https://doi.org/10.1016/j.earscirev.2019.03.012

Tait, J.A., Bachtadse, V., Franke, W. and Soffel, H.C. 1997. Geodynamic evolution of the European Variscan fold belt: palaeomagnetic and geological constraints. *Geologische Rundschau*, **86**, 585–598, https://doi.org/10.1007/s005310050165

Toyos, J.M. and Aramburu-Zabala, C.I. 2014. El Ordovícico en el área de Los Barrios de Luna, Cordillera Cantábrica (NW de España). *Trabajos de Geología, Universidad de Oviedo*, **34**, 61–96, https://doi.org/10.17811/tdg.34.2014.61-96

Valverde-Vaquero, P. and Dunning, G.R. 2000. New U–Pb ages for Early Ordovician magmatism in central Spain. *Journal of the Geological Society*, **157**, 15–26, https://doi.org/10.1144/jgs.157.1.15

Vermeesch, P. 2012. On the visualisation of detrital age distributions. *Chemical Geology*, **312**, 190–194, https://doi.org/10.1016/j.chemgeo.2012.04.021

Vermeesch, P. 2013. Multi-sample comparison of detrital age distributions. *Chemical Geology*, **341**, 140–146, https://doi.org/10.1016/j.chemgeo.2013.01.010

Vermeesch, P. 2017. Dissimilarity measures in detrital geochronology. *Earth-science Reviews*, **178**, 310–321, https://doi.org/10.1016/j.earscirev.2017.11.027

Vermeesch, P. 2018. IsoplotR: a free and open toolbox for geochronology. *Geoscience Frontiers*, **9**, 1479–1493, https://doi.org/10.1016/j.gsf.2018.04.001

Weil, A.B. 2006. Kinematics of orocline tightening in the core of an arc: paleomagnetic analysis of the Ponga Unit, Cantabrian Arc, northern Spain. *Tectonics*, **25**, https://doi.org/10.1029/2005TC001861

Weil, A.B., Gutierrez-Alonso, G. and Conan, J. 2010. New time constraints on lithospheric-scale oroclinal bending of the Ibero-Armorican Arc: a palaeomagnetic study of earliest Permian rocks from Iberia. *Journal of the Geological Society*, **167**, 127–143, https://doi.org/10.1144/0016-76492009-002

Weil, A.B., Gutiérrez-Alonso, G., Johnston, S.T. and Pastor-Galán, D. 2013. Kinematic constraints on buckling a lithospheric-scale orocline along the northern margin of Gondwana: a geologic synthesis. *Tectonophysics*, **582**, 25–49, https://doi.org/10.1016/j.tecto.2012.10.006

Weil, A.B., Pastor-Galán, D., Johnston, S.T. and Gutiérrez-Alonso, G. 2019. Late/post Variscan orocline formation and widespread magmatism. *In*: Quesada, C. and Oliveira, J.T. (eds) *The Geology of Iberia: A Geodynamic Approach*. Springer, Chamonix, Regional Geology Reviews, **2**, 527–542. https://doi.org/10.1007/978-3-030-10519-8_14

Wissink, G.K., Wilkinson, B.H. and Hoke, G.D. 2018. Pairwise sample comparisons and multidimensional scaling of detrital zircon ages with examples from the North American platform, basin, and passive margin settings. *Lithosphere*, **10**, 478–491, https://doi.org/10.1130/L700.1

Woodcock, N.H., Soper, N.J. and Strachan, R.A. 2007. A Rheic cause for the Acadian deformation in Europe. *Journal of the Geological Society*, **164**, 1023–1036, https://doi.org/10.1144/0016-76492006-129

Žák, J. and Sláma, J. 2018. How far did the Cadomian 'terranes' travel from Gondwana during early Palaeozoic? A critical reappraisal based on detrital zircon geochronology. *International Geology Review*, **60**, 319–338, https://doi.org/10.1080/00206814.2017.1334599

Zimmermann, U., Andersen, T., Madland, M.V. and Larsen, I.S. 2015. The role of U–Pb ages of detrital zircons in sedimentology – An alarming case study for the impact of sampling for provenance interpretation. *Sedimentary Geology*, **320**, 38–50, https://doi.org/10.1016/j.sedgeo.2015.02.006